UNIVERSIDAD NACIONAL AUTÓNOMA DE MÉXICO
MAESTRÍA EN CIENCIAS (FÍSICA)
FÍSICA CUÁNTICA, ATÓMICA Y MOLECULAR

Optical cavity prototype for Rydberg quantum optics experiments

TESIS
QUE PARA OPTAR POR EL GRADO DE:
Maestro

PRESENTA:
Leonardo Uhthoff Rodríguez

DIRECTOR DE TESIS
Dr. Asaf Paris Mandoki
IF, UNAM
COMITÉ TUTOR
Dra. Karen Patricia Volke Sepúlveda
IF, UNAM
Dr. Pablo Barberis Blostein
IIMAS, UNAM

CIUDAD DE MÉXICO, DICIEMBRE, 2022

JURADO ASIGNADO:

Sinodal 1:	Dr. Giuseppe Pirruccio
Sinodal 2:	Dra. Martha Rosete Aguilar
Sinodal 3:	Dr. Pedro Antonio Quinto Su
Sinodal 4:	Dr. Jesús Garduño Mejía
Sinodal 5:	Dr. Asaf Paris Mandoki

DIRECTOR DE TESIS:

Dr. Asaf Paris Mandoki

_____

Agradecimientos

El primer agradecimiento le corresponde a mi asesor el Dr. Asaf Paris quien me ha instruido desde mi servicio social de la licenciatura y siempre me guió en este proyecto con mucho entusiasmo y disposición. Después a mis compañeros y grandes amigos, Eduardo Esquivel y Giovanni Alonso, que han hecho esto posible con su valioso trabajo en el laboratorio junto con todos los demás estudiantes y colaboradores del Laboratorio de Óptica Cuántica de Rydberg dentro de los cuales destacan los electrónicos Carlos Gardea que desarrolló gran parte de la instrumentación utilizada en este proyecto, Rodrigo Gutiérrez por sus numerosas asesorías técnicas y al Dr. Jorge Seman que muy atentamente nos facilitó material que resultó indispensable para la realización del proyecto. Aprecio mucho también a la Dra. Judith Campos y de nuevo a Asaf que me permitieron participar en las ayudantías de sus cursos, mientras realizaba la maestría.

Fuera de lo académico he recibido apoyo de muchas personas entre las cuales destacan mis papás, mi hermano y mi amada Jazmín a las cuales quiero darles muchas gracias por siempre escucharme y ayudarme. Tmbién a mis amigos Marcos Bermúdez, Jorge Cruz, Eduardo Esquivel, Alonso Sandoval, Alvar Ortega y Sergio Ortiz que sé que seguirán ahí en mi futuro.

Agradezco también a los miembros del C.C.P. por todas los entretenidos momentos a la hora de la comida, parrilladas y festivales.

Por último un agradecimiento a las instituciones que han financiado el proyecto del Laboratorio de Óptica Cuántica de Rydberg dentro del cual se desarrolló la presente investigación:
Instituto de Física, UNAM.
DGAPA-UNAM, PAPIIT:IA104220
Coordinación de la Investigación Científica UNAM: LANMAC-2020, LANMAC-2021, LANMAC-2022
CONACYT:
- Investigación Científica Básica A1-S-29630
- Laboratorio Nacional:299057, 314860, 315838.
- Programa de becas nacionales para estudios de posgrado.

A Miguel...

Abstract/Resumen

In this thesis, we implement a Fabry-Perot type optical cavity with spherical mirrors of 5 cm radius of curvature in a near concentric configuration. This prototype has the objective of helping the future development of a resonator that serves to enhance light-matter coupling in a cold Rydberg atoms experiment. The near concentric configuration is close to being an unstable resonator so a study of the requirements to build such a cavity is done. We include a description of how to match the cavity mode and a method for alignment. For characterization, we undertake measurements of cavity length by means of the free spectral range, cavity waist using the Gouy phase, and we also determine linewidth and finesse. Lastly, we explain the Pound-Drever Hall method to lock cavity length. As a conclusion, an analysis is done of the most important aspects that will be needed in the future for the implementation of the cavity, which will be inside the vacuum system where the Rydberg cold atoms experiments are conducted.

En la presente tesis se realiza un prototipo de cavidad óptica tipo Fabry-Perot con espejos esféricos de 5 cm de radio de curvatura en configuración casi concéntrica. Este prototipo tiene como objetivo ayudar a desarrollar un resonador que sirva para mejorar el acoplamiento luz-materia en un experimento de átomos fríos de Rydberg. En la configuración casi concéntrica la cavidad está cerca de ser inestable por lo que se estudia qué necesidades hay que cumplir para poder construir un resonador de este tipo. Se describe cómo se ajusta el modo en la cavidad y un método para alinearla. Para caracterización se realizan mediciones de la longitud de la cavidad por medio del rango espectral libre, medición de la cintura a partir de la fase de Gouy, y la determinación del ancho de línea y fineza. Por último se desarrolla y aplica el método de Pound Drever Hall para anclar la longitud de la cavidad. Como conclusión se analizan los aspectos más importantes que se necesitarán a futuro para la realización de la cavidad que irá dentro del sistema de vacío donde se conducen los experimentos con átomos fríos de Rydberg.

Contents

Introduction

Cold atoms experiments provide a very precise way to study the quantum mechanical properties of matter and have a large variety of applications including quantum simulation [1, 2], quantum metrology [3] and quantum computation [4]. Laser cooling was first proposed in 1975 [5, 6] eventually a lot of progress was made possible in this area thanks to the development of laser systems which allowed the first optical molasses, this confinement was first demonstrated experimentally in 1985 [7] and was awarded the Nobel Prize in Physics in 1997. This experimental techniques rely on the confinement of an atomic gas by means of a light beam array which in combination with a controlled magnetic field apply a frictional-style force by means of radiation pressure to the atoms, slowing them towards the center of the array. A very interesting field which can be explored with this systems is the study of light matter interaction, which can be amplified by confining the atoms within an optical cavity. When doing this the coupling between light and matter may become very strong and the whole system acts as a coupled oscillator [8].

This phenomena can be divided in two domains, first the "low-Q cavity" regime in which the photons emitted by the atoms are very rapidly and irreversibly dissipated in the cavity walls and the "high-Q cavity regime", the photons are stored within the cavity walls enough time so that they interact coherently with the atom [9]. In this work we study a prototype for a cavity of the first kind, this type of system has a fast response compared to the atomic dynamics so measuring the cavity transmission serves as a real time monitor of the atomic system excitations and also the presence of a resonator enhances coupling of light with atoms allowing interaction at lower laser power inputs.

The atomic system for which the cavity is planned is a Rydberg atoms experiment. Rydberg atoms provide a great medium to explore and mediate the interaction between light and matter, they are defined as atoms in states of high principal quantum number, n, this condition provides exaggerated properties which scale with n as shown in Table 1. Because of this, many applications have been found [10, 11], which exploit their long lifetimes and great polarizability.

Of particular interest in quantum optics, quantum information and as a motivation for this work is a phenomena called Rydberg atom dipole blockade or better explained

Property	n-scaling	$^{87}Rb(100s_{1/2})$
Orbital radius	n^2	$0.96\,\mu m$
Radiative lifetime	n^3	$1.24\,ms$
Polarizability	n^7	$6.25\,GHz(V/cm)^{-2}$
van der Waals C_6	n^{11}	$56.4\,THz/\mu m^6$

Table 1: Scaling properties of Rydberg atoms [12]

as the inhibition of multiple Rydberg excitations. It arises from a van der Waals-like potential corresponding to a second order dipole-dipole interaction between two atoms. This interaction becomes relevant when dealing with highly excited atoms because of their huge dipole matrix elements. For a pair of atoms the dipole-dipole interaction operator takes the usual form [13]:

$$V_{\mathrm{dd}}(\mathrm{R}) = \frac{\hat{\mathbf{d}}_1 \cdot \hat{\mathbf{d}}_2 - 3(\hat{\mathbf{n}} \cdot \hat{\mathbf{d}}_1)(\hat{\mathbf{n}} \cdot \hat{\mathbf{d}}_2)}{\mathrm{R}^3}, \tag{1}$$

where R is the inter-atomic distance, $\hat{\mathbf{n}} = \mathbf{R}/\mathrm{R}$ is the normal vector pointing from one atom to the other and $\hat{\mathbf{d}}_i$ is the dipole operator $e\hat{\mathbf{r}}_\mathrm{i}$ for each atom.

When R is large so that the individual atomic wave functions do not overlap, the interaction term of equation (1) might be treated as a perturbation. To first order perturbation theory the contribution is zero since the dipole operator does not couple same parity states so second order perturbation theory is considered. The energy correction is calculated to be [13]:

$$\Delta E = \sum_{i,k} \frac{|\langle i;k|\mathrm{V}_{\mathrm{dd}}(R)|1;2\rangle|^2}{E_{1,2} - E_{i,k}}, \tag{2}$$

where i and k run over states dipole-coupled to $|1\rangle$ and $|2\rangle$. The factor $1/R^3$ can go out from the sum and the above equation is then written as

$$\Delta E = \frac{C_6(\theta)}{R^6}, \tag{3}$$

where θ is the angle between the inter-atomic axis and the quantization axis and arises when considering the angular momentum quantum numbers [14]. Equation (3) is a Van der Waals like interaction for large distances between atoms. To excite an atom to a Rydberg level, it is necessary to irradiate it with light whose frequency corresponds to that of the atomic transition. To excite two atoms, usually the same frequency would excite them. However, when exciting to a Rydberg level, the Van der Waals interaction

shifts the frequency needed to produce a second excitation when atoms are close enough to each other. This phenomena is called the Rydberg blockade. It means there is a volume defined by an inter-atomic distance called the blockade radius R_b where the energy shift (equation (3)) is such that the simultaneous excitation of more than one atom is forbidden. A diagram of this situation is depicted on Figure 1. When an entire atomic cloud fits within the blockade volume this collective behaves as a single two-level system because only one excitation is allowed within the sample. This increases the effective cross section of the atoms improving atom-light coupling.

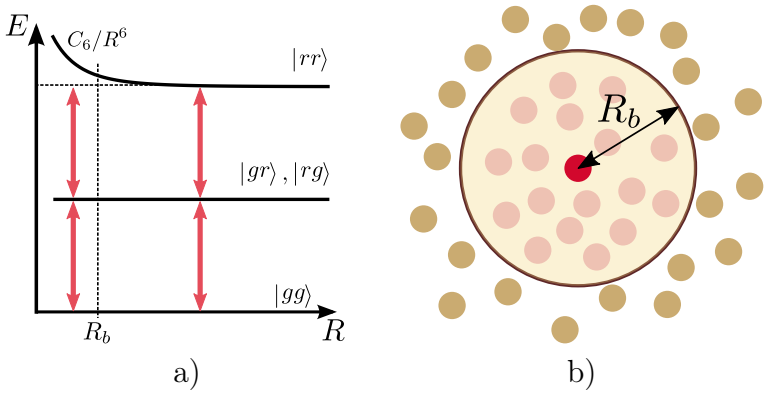

Figure 1: a) The system composed of a pair of two level atoms can be excited using a single laser frequency (depicted in red) to level $|rr\rangle$ when their interatomic distance R is greater then R_b. However when $R < R_b$ this becomes impossible due to a Van der Waals like interaction which shifts the energy level. Level $|g\rangle$ is considered to be a ground state and level $|r\rangle$ is a Rydberg state. b) Atoms within a blockade radius from a Rydberg excited atom can not be simultaneously excited to a Rydberg level. The system within the blockade volume acts as an effective two level atom with enhanced coupling to the light field and is called the Rydberg superatom.

Secondly the resonator and atom system is described by the Jaynes-Cummings model [15], which is a quantum description of both a single two level atom interacting with a quantized single mode field. This model considers the interaction in the electric dipole approximation, the dipole operator for the atom can be written as $\hat{\mathbf{d}} = \mathbf{d}_{eg}(\hat{\sigma}_{eg} + \hat{\sigma}_{ge})$ where $\mathbf{d}_{eg}$ is the dipole matrix element $-q\langle e|\hat{\mathbf{r}}|g\rangle$, $\hat{\sigma}_{eg} = |e\rangle\langle g|$ and $\hat{\sigma}_{eg} = \hat{\sigma}_{ge}^{\dagger}$. The quantized single electric field mode is $\hat{\mathbf{E}} = \mathbf{f}\sqrt{\hbar\omega_c/\epsilon_0 V}(\hat{a}^{\dagger} + \hat{a})$ where $\mathbf{f}$ is the mode envelope, V the mode volume and ω_c the cavity resonant frequency. Then the interaction hamiltonian is written as:

$$\hat{H}_{\text{int}} = -\hat{\mathbf{d}} \cdot \hat{\mathbf{E}} = \hbar g_0(\hat{a}^{\dagger} + \hat{a})(\hat{\sigma}_{eg} + \hat{\sigma}_{ge}), \tag{4}$$

The constant g_0 characterizes the interaction strength and thus is called the coupling constant, it is proportional to the dipole matrix element $\mathbf{d}_{eg}$ projected over the mode envelope $\mathbf{f}$ and inversely proportional to the square root of the effective mode volume V:

$$g_0 = \sqrt{\frac{\omega_c}{2\epsilon_0 V\hbar}}\mathbf{d}_{eg} \cdot \mathbf{f}, \tag{5}$$

A generalization for an atom-cavity system with N atoms is the open Tavis-Cummings model [16] which in the limit of small number of excitations shows the atomic ensemble has a collective behavior as a harmonic oscillator and the coupling between two level atoms and light is as two coupled harmonic oscillators. In this situation light matter interaction is amplified by the number of atoms with coupling constant $g_{coll} = g_0\sqrt{N}$, then an enhanced coupling to the light is obtained.

The three topics mentioned above serve as the motivation for the present work. It is about the design and construction of a Fabry Perot type cavity, which helps for the future implementation of a cavity inside a Rydberg atoms experiment. The future purpose for the cavity will be to enhance light-matter interactions and to support a highly focused beam so that it creates a single Rydberg blockade volume within an atomic cloud. The main issues which are covered are, the practical limitations of a near-concentric cavity, the minimum waist obtainable, how to measure it, and how to lock the cavity length using the Pound Drever Hall method.

Outline of the thesis

Chapter 1 is a theoretical introduction to the Fabry-Perot type cavities. In particular to the symmetric and near concentric ones.

Chapter 2 presents the experimental aspects of how the resonator components where selected and how the optical arrangement was constructed in order to ensure proper alignment and coupling to the resonant modes of the cavity.

Chapter 3 is about measurements done to characterize the cavity. It has the methods used and the results obtained from the cavity length, waist, and finesse measurements.

Chapter 4 is an overview of the Pound Drever Hall method and how it was implemented to generate an error signal to lock the cavity length.

Chapter 5 describes the conclusions of this thesis, including the important aspects to take into account for a future design of the cavity.

Chapter 1

Resonant Optical Cavities

An optical resonator is an optical circuit in which light is confined [17]. There is a large variety of them, the simplest of these is the Fabry-Perot which consists of two plane parallel mirrors facing each other so that light is reflected multiple times between them experiencing little loss and interfering with itself forming standing waves. The next simplest variation of the Fabry-Perot resonator is adding a radii of curvature R_1 and R_2 to the mirrors, this parameters together with the spacing between them L are enough to create a wide variety of resonators which will be studied in this chapter. However there exist an even larger set of ways of storing light in optical resonators such as ring configurations of mirrors, rectangular cavities, fiber rings, microdisks, microtoroids, spheres and so on. In this thesis we focus on spherical mirror resonators.

1.1 The Basics of Spherical Mirror Resonators

The simplest approach for solving the problem of light confinement between two spherical mirrors facing each other is based on ray optics. The resonator is constructed using two spherical mirrors of radii R_1 and R_2 with separation distance L (Figure 1.1), and is then analyzed as a periodical optical system, since it repeats itself after two reflections, using ABCD matrices [18]. The result gives a stability criteria which tells the parameters for light to get trapped in the resonator.

A method that provides the same result for spherical mirror resonators is to use

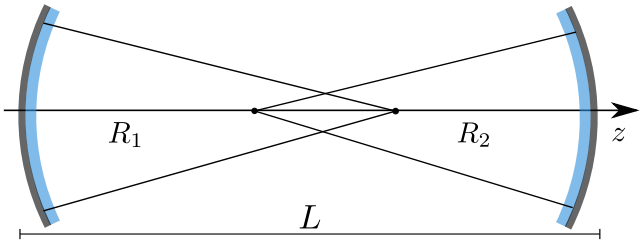

Figure 1.1: Resonator configuration. R_1 and R_2 are the radii of curvature of the mirrors and L is the resonator length, i.e. the distance between mirrors.

beam optics. In particular given the resonator geometry we need a beam that retraces itself after reflecting from the mirrors, for this it is necessary to discuss the Gaussian beams.

1.1.1 Gaussian Beams

We start by making an approximation to the Helmholtz equation which is [18]:

$$\nabla^2 U + k^2 U = 0, \tag{1.1}$$

where k is the wavenumber and U is the complex amplitude of the wave. A light beam has the porperties of being spatially confined and travel in space without diverging, so it is imposed to the solution that [18]:

$$U(\mathbf{r}) = A(\mathbf{r}) e^{-ikz}. \tag{1.2}$$

This is like a plane wave but it has an envelope $A(\mathbf{r})$ that varies slowly, within the scale of a wavelength, with position z. Then it is guaranteed the beam travels in space without diverging and is known as the paraxial condition, which turns out can be expressed as [18]:

$$\frac{\partial^2 A}{\partial z^2} \ll k^2 A. \tag{1.3}$$

Substituting (1.2) into (1.1) and neglecting $\frac{\partial^2 A}{\partial z^2}$ we obtain the paraxial Helmholtz equation:

$$\nabla_T^2 A - i2k \frac{\partial A}{\partial z} = 0, \tag{1.4}$$

where $\nabla_T^2 = \frac{\partial^2}{\partial x^2} + \frac{\partial^2}{\partial y^2}$.

By solving equation (1.4) different beam-like solutions can be obtained depending on the chosen coordinate system. In particular we focus on two sets of solutions, each of them forming a complete basis. They will become relevant in section 2.4 when the resonator alignement is considered. First in cartesian coordinates, using the Hermite-Gauss functions of order l [18]:

$$\mathbb{G}_l(u) = \mathbb{H}_l(u) \exp\left\{\frac{-u^2}{2}\right\},\ l = 0, 1, 2, \tag{1.5}$$

with $\mathbb{H}_l(u)$ the Hermite polynomials, the set of solutions for the beam complex amplitude are [18]:

$$U_{l,m}(x,y,z) = A_{l,m}\left[\frac{\omega_0}{\omega(z)}\right]\mathbb{G}_l\left[\frac{\sqrt{2}x}{\omega(z)}\right]\mathbb{G}_m\left[\frac{\sqrt{2}y}{\omega(z)}\right]\exp\left\{-ikz - ik\frac{x^2+y^2}{2R(z)} + i(l+m+1)\zeta(z)\right\}, \tag{1.6}$$

where $A_{l,m}$ is a constant and the following beam parameters are defined as:

Gaussian beam parameters

$$\omega(z) = \omega_0\sqrt{1+\left(\frac{z}{z_0}\right)^2}, \qquad \text{(Beam waist)} \tag{1.7a}$$

$$R(z) = z\left[1+\left(\frac{z_0}{z}\right)^2\right], \qquad \text{(Beam radius)} \tag{1.7b}$$

$$\zeta(z) = \tan^{-1}\frac{z}{z_0}, \qquad \text{(Gouy phase)} \tag{1.7c}$$

$$\omega_0 = \sqrt{\frac{\lambda z_0}{\pi}}. \qquad \text{(waist and Rayleigh range relation)} \tag{1.7d}$$

The second complete set of solutions is obtained solving the paraxial Helmholtz equation in cylindrical coordinates (ρ, ϕ, z). In this case the complex amplitude is in terms of the generalized Laguerre polynomial function $\mathbb{L}_m^l$ and is called the Laguerre-Gauss beam. Its formula is expressed as:

$$\begin{aligned} U_{l,m}(x,y,z) = A_{l,m}&\left[\frac{\omega_0}{\omega(z)}\right]\left(\frac{\rho}{\omega(z)}\right)^l\mathbb{L}_m^l\left[\frac{2\rho^2}{\omega^2(z)}\right]\exp\left\{-\frac{\rho^2}{\omega^2(z)}\right\} \\ &\times\exp\left\{-ikz - ik\frac{\rho^2}{2R(z)} - il\phi + j(l+2m+1)\zeta(z)\right\}, \end{aligned} \tag{1.8}$$

where $\omega(z)$, $R(z)$, $\zeta(z)$ and W_0 are the beam parameters defined in equations (1.7). Figure 1.2 shows the intensity distributions $I = |U|^2$ for the Hermite-Gauss and Laguerre-Gauss beams at $z = 0$ and different orders (l, m). In both cases the $(0, 0)$ order is the same and it is known as the gaussian beam.

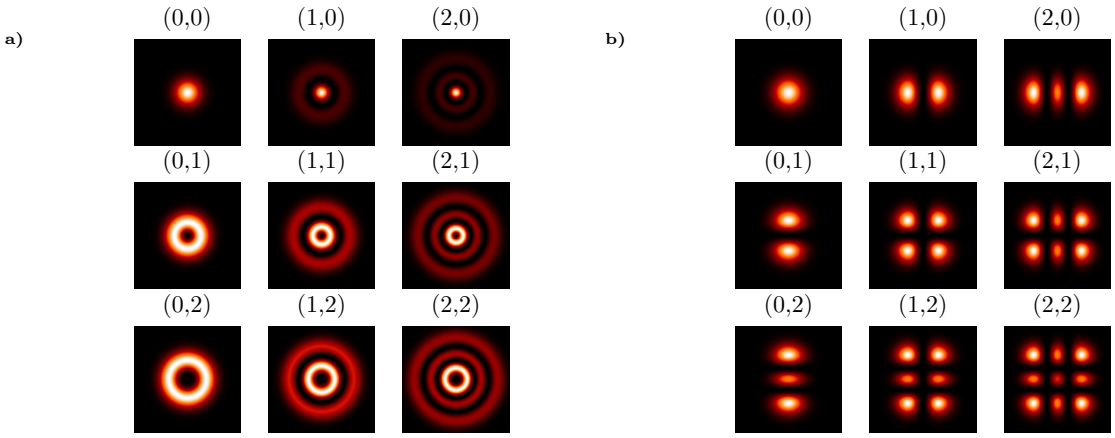

Figure 1.2: a) Laguerre-Gaussian (l, m) and b) Hermite-Gaussian (l, m) transverse intensity profiles for $z = 0$.

The optical intensity is $I(\mathbf{r}) = |U(\mathbf{r})|^2$ and its integration over any transverse plane yields the total power. For the gaussian beam turns out to be half the peak intensity $I_0 = |A_{0,0}|^2$ multiplied by the beam area $\pi\omega_0^2$. When comparing this total power with the power obtained from the integration of intensity within a circle with radius equal to the beam waist $\omega(z)$ it turns out 86% of the beam power is carried within this circle. The function for the beam waist asumes its minimum value at $z = 0$ and increases for positive and negative z as indicated by equation (1.7a). The parameter z_0 is called the Rayleigh range and $2z_0$ is the region around the origin where the beam diverges maximum $\sqrt{2}\omega_0$, for this reason is known as the depth of focus or the confocal parameter. The phase of a gaussian beam is

$$\phi(r, z) = ikz + i\zeta(z) - ik\frac{\rho^2}{2R(z)}, \tag{1.9}$$

where

$$\zeta(z) = \arctan\left(\frac{z}{z_R}\right). \tag{1.10}$$

The first term of equation (1.9) corresponds to a plane wave, then it has an additional term known as the Gouy phase $\zeta(z)$ which adds an extra $\pm\pi/2$ phase around the beam waist. The third term is parabolic in the radius and decribes how the wavefronts

bend around its focus. The wavefronts are the surfaces of constant phase which turn out to be paraboloidal surfaces with radius $R(z)$ under the assumption that the radius of curvature $R(z)$ and the Gouy phase $\zeta(z)$ are slowly varying functions of z. A schematic of the Gaussian beam showing its waist, wavefronts and Gouy phase is depicted in Figure 1.3.

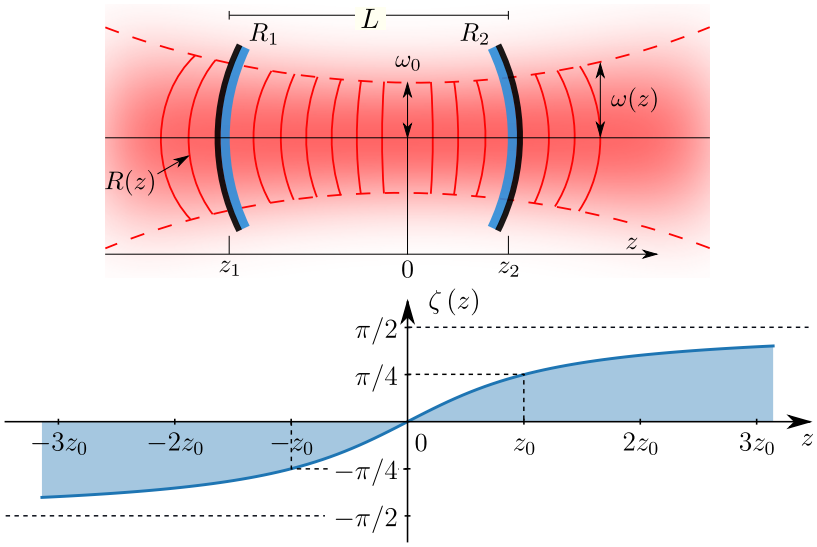

Figure 1.3: Above is a transverse cut of a gaussian beam, its characteristics and resonator mirrors matching the paraboloidal wavefronts. Below is depicted the Gouy phase shift.

1.1.2 Modes in a Spherical Resonator

Now lets think on fitting a gaussian beam so that the waist lies somewhere inside the resonator and its paraboloidal wavefronts match the radii of curvature of the spherical mirrors. If this happens the gaussian beam would be trapped as a standing wave under the assumption that the mirrors are large enough compared to the beam size so that the paraxial approximation remains valid and the losses by diffraction are negligible.

Following this reasoning it is assumed that the mirrrors are located at unknown distances z_1 and z_2 from the beam waist ω_0, but restricted to match the cavity length L, and that the wavefront curvature $R(z)$ is fixed by the mirror's radii of curvature R_1 and R_2, this conditions are written as

$$R(z_1) = z_1 + z_R^2/z_1 = -R_1, \tag{1.11a}$$

$$R(z_2) = z_2 + z_R^2/z_2 = +R_2, \tag{1.11b}$$

$$L = z_2 - z_1. \tag{1.11c}$$

Equations (1.11) turn out to be enough for determining all gaussian beam parameters from equations (1.7). Defining g_1 and g_2 called the resonator g parameters as:

$$g_1 = 1 - \frac{L}{R_1}, \tag{1.12a}$$

$$g_2 = 1 - \frac{L}{R_2}, \tag{1.12b}$$

the gaussian beam is characterized as follows [19]:

Gaussian beam properties that match a given cavity configuration

$$z_R^2 = \frac{g_1 g_2 (1 - g_1 g_2)}{g_1 + g_2 - 2 g_1 g_2} L^2, \quad \text{(Rayleigh range)} \tag{1.13a}$$

$$z_1 = \frac{g_2 (1 - g_1)}{g_1 + g_2 - 2 g_1 g_2} L, \quad \text{(Mirror } R_1 \text{ location)} \tag{1.13b}$$

$$z_2 = \frac{g_1 (1 - g_2)}{g_1 + g_2 - 2 g_1 g_2} L, \quad \text{(Mirror } R_2 \text{ location)} \tag{1.13c}$$

$$\omega_0^2 = \frac{L\lambda}{\pi} \sqrt{\frac{g_1 g_2 (1 - g_1 g_2)}{(g_1 + g_2 - 2 g_1 g_2)^2}}, \quad \text{(Beam waist)} \tag{1.13d}$$

$$\omega_1^2 = \frac{L\lambda}{\pi} \sqrt{\frac{g_2}{g_1 (1 - g_1 g_2)}}, \quad \text{(Beam waist at mirror } R_1) \tag{1.13e}$$

$$\omega_2^2 = \frac{L\lambda}{\pi} \sqrt{\frac{g_1}{g_2 (1 - g_1 g_2)}}. \quad \text{(Beam waist at mirror } R_2) \tag{1.13f}$$

There are some g_1 and g_2 parameters that make equations (1.13a-1.13f) imaginary or infinite, this means there is no gaussian beam solution whose wavefronts match the radius of curvature of the mirrors given the resonator length. When this happens, we say the optical cavity is not stable, the condition for stability guarantees the mentioned equations are real and finite, it is given by:

$$0 \leq g_1 g_2 \leq 1. \tag{1.14}$$

This inequality is also found in ray optics when using a matrix periodic system analysis, meaning that given this conditions there exist rays that will be trapped within cavity mirrors. Expression (1.14) can be better understood looking at Figure 1.4 which depicts the stability region and positions of different resonator configurations. The most stable configuration is located at the origin because moving the parameters along the identity line keeps the cavity stable, this turns out to be when g_1 and g_2 equal zero which means mirrors with same radii of curvature are placed with distance L between them such that their focuses match in the center of the resonator and therefore is called a confocal cavity.

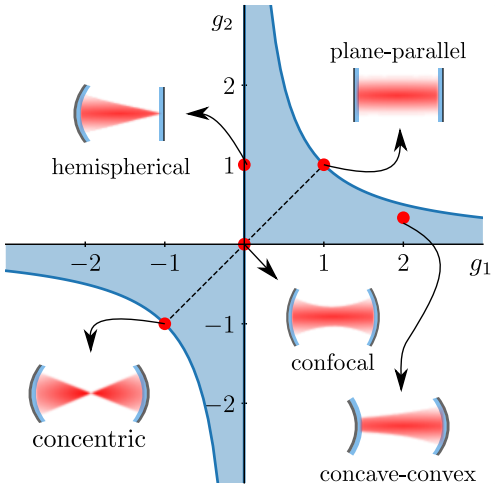

Figure 1.4: Spherical resonator stability diagram. The dashed line corresponds to the parameter space of symmetric resonators.

1.2 The Near Concentric Resonator

The stability diagram (Figure 1.4) shows different configurations which have different applications. However, the main interest in this work is achieving the minimum waist posible so that only one Rydberg blockade volume can be excited within the cold atomic cloud. This configuration corresponds to the concentric one, in which equal mirrors are appart from each other by two times their radii of curvature.

1.2.1 Symmetric Resonators

In this case the resonator g parameters are equal, this means both mirrors have the same radius of curvature R and the minimum waist is achieved at the center of the cavity. Then equation (1.14) reduces to $g^2 \leq 1$ with $g = g_1 = g_2 = 1 - L/R$ and equations (1.7a-1.13f) simplify to

$$w_0^2 = \frac{L\lambda}{\pi}\sqrt{\frac{1+g}{4(1-g)}}, \qquad (1.15a) \qquad w_1^2 = w_2^2 = \frac{L\lambda}{\pi}\sqrt{\frac{1}{1-g^2}}. \qquad (1.15b)$$

Using equations (1.15) we can now examine the effect of varying the mirrors radius R for a fixed distance between mirrors L. Which is the same as moving the g parameter in the stability diagram along the identity line from $(1, 1)$ to $(-1, -1)$, this is shown in Figure 1.5. When $g = 1$ the radii of the mirrors must be infinite, this is the planar case and the beam width at the waist, w_0, and at the mirrrors, $w_1 = w_2$, also diverges. When $g = 0$ or $L/R = 1$ is the confocal configuration located at the center of the stability diagram, in this case the waist at the mirrors attains its minimum size compared to the focus waist and it turns out to be $\sqrt{2}w_0$. It means the depth of focus $2z_0$ is equal to the length of the

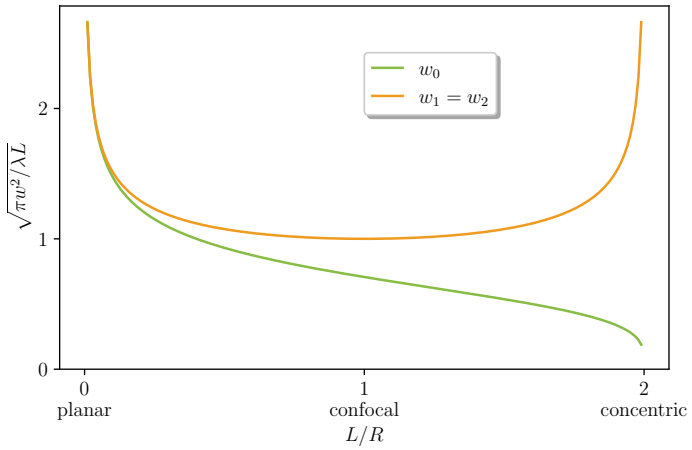

Figure 1.5: Plot of equations 1.15. Vertical axis is selected in such a way to represent adimensional waist variation. The horizontal axis is better understood as the variation of R when L is fixed to an arbitrary constant. The plot shows the behaviour of beam waist at the center of the resonator, ω_0, and at the mirrors, $\omega_1 = \omega_2$, when moving from the planar to the concentric situtation.

resonator L. Lastly $g = -1$ or $L/R = 2$ is the concentric configuration, while the waist w_0 goes to zero the waist at the mirrors becomes infinite. This limit is physically impossible and that is why we are interested on getting as close as possible to the concentric regime without reaching it. Because the waist ω_0 can be arbitrarily small we will focus in the case of near-concentric resonators.

1.2.1.1 Near Concentric Resonators

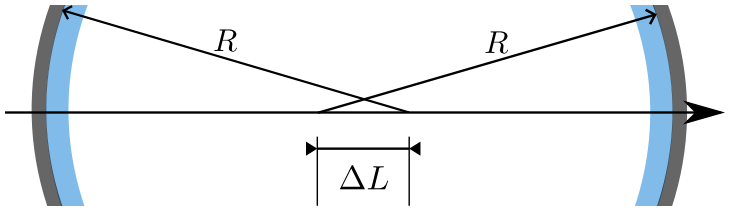

Figure 1.6: Near concentric resonator

As it has been discussed previously this cavity houses a very focused gaussian mode, where the cavity waist can be on the order of μm, as caculated later in the text (Chapter 2). This would not be very useful in the case of laser power extraction where the cavity mode interacts with a large lasing medium [19]. However, the purpose of this cavity is for the light within to interact with a cold atom cloud also in the order of μm, so the fact of the cavity field being concentrated in a size comparable to the cross section of the atomic medium will offer a strong interaction.

A reasonable way to characterize this type of resonator is by how far it is to concentric, then we introduce the parameter ΔL which will be the small ammount needed for the distance between mirrors to be exactly two times the radius of curvature. Now the

cavity length is $L = 2R - \Delta L$, in consequence the resonator g parameter is $g = -1 + \Delta L/R$. Substituting this, $R = (L + \Delta L)/2$ and using the approximation $\Delta L \ll L$ into equations (1.15) then:

$$w_0^2 = \frac{L\lambda}{\pi}\sqrt{\frac{\Delta L}{4L}}, \qquad (1.16a) \qquad w_1^2 = w_2^2 \approx \frac{L\lambda}{\pi}\sqrt{\frac{L}{4\Delta L}}. \qquad (1.16b)$$

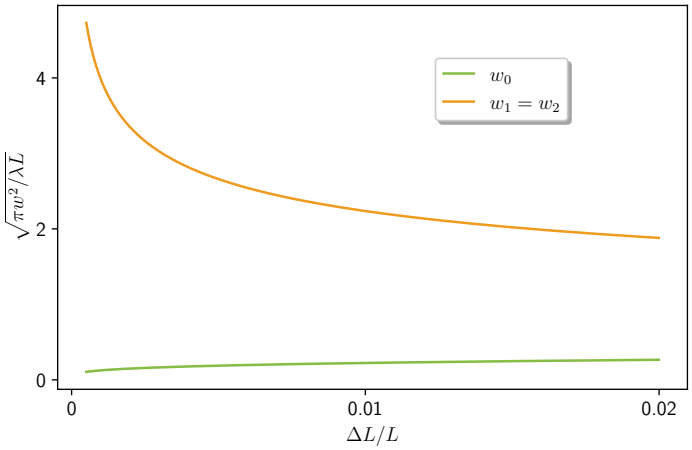

Figure 1.7: Near concentric resonator. Plot of equations 1.16. Vertical axis is selected in such a way to represent adimensional waist variation. When moving appart from the near concentric situation the plot shows how the beam waist at the center of the resonator, ω_0, is near zero and presents a small change compared to the waist at the mirrors, $\omega_1 = \omega_2$ which diminishes rapidly.

1.3 Cavity Spectra, Losses and Spectral Width

This section describes the condition for light frequency to be resonant with the cavity mode, and the connection between cavity losses and the spectral width.

1.3.1 Cavity Spectra

A gaussian beam was considered to be a resonant mode of an spherical cavity under the assumption that its wavefronts match the radius of curvature of the mirrors, this means the wavefront normals will reflect back onto themselves following the same path and also the phase would retrace itself. Since we know the phase of the gaussian beam, The phase of an Hermite-Gauss beam of order (l, m) at points on the optical axis ($\rho = 0$) can be retrieved from equation (1.6) as:

$$\phi(0, z) = kz - (l + m + 1)\zeta(z). \qquad (1.17)$$

This will help to establish the resonant light frequencies in the cavity. Then the acquired phase when the beam travels from one mirror to the other is:

$$\begin{aligned}\phi(0,z_2)-\phi(0,z_1) &= k(z_2-z_1)-(l+m+1)[\zeta(z_2)-\zeta(z_1)] \\ &= kL-(l+m+1)\Delta\zeta.\end{aligned} \tag{1.18}$$

The condition for the beam to fully retrace itself, means that after a round trip the phase change must be equal to zero or a multiple of $\pm 2\pi$ then

$$2kL-2(l+m+1)\Delta\zeta = 2\pi q, \tag{1.19}$$

where $q = 0, \pm 1, \pm 2, ...$

Substituting $\nu_F = c/2L$ and $k = 2\pi\nu/c$ the resonance frequencies for Hermite-Gauss beams are given by:

$$\nu_{l,m,q} = q\nu_F + (l+m+1)\frac{\Delta\zeta}{\pi}\nu_F. \tag{1.20}$$

In an analog way the resonance frequencies for different Laguerre-Gauss modes (l, m) are:

$$\nu_{l,m,q} = q\nu_F + (l+2m+1)\frac{\Delta\zeta}{\pi}\nu_F. \tag{1.21}$$

The frequency spacing between two different transverse Hermitte-Gauss (l, m) and (l', m') modes which correspond to the same longitudinal mode q is in consequence

$$\nu_{l,m,q} - \nu_{l',m',q} = [(l+m)-(l'+m')]\frac{\Delta\zeta}{\pi}\nu_F, \tag{1.22}$$

and between the same transverse (l, m), but different longitudinal adjacent $\nu_{l,m,q}$ and $\nu_{l,m,q+1}$ modes is:

$$\nu_F = \frac{c}{2L}, \tag{1.23}$$

which is known as the free spectral range.

The term $\Delta\zeta$ is the acquired Gouy phase from one mirror to another mirror this

means:

$$\Delta\zeta = \arctan\left(\frac{z_2}{z_R}\right) - \arctan\left(\frac{z_1}{z_R}\right), \tag{1.24}$$

however it can be written after some algebra [19] in terms of the g parameters as:

$$\Delta\zeta = \arccos \pm\sqrt{g_1 g_2}, \tag{1.25}$$

where the $+$ sign is for $g_1, g_2 > 0$ and the $-$ sign when $g_1, g_2 < 0$ (see Figure 1.4). From this we inmediatly know the value of $\Delta\zeta/\pi$ for the different symmetric resonator configurations, i.e. along the identity line in the stability diagram. This is shown in the following table:

Cavity configuration	g_1,g_2	$\Delta\zeta/\pi$
near-planar	~ 1	~ 0
near-confocal	~ 0	$\sim 1/2$
near-concentric	~ -1	~ 1

Table 1.1: Gouy phase shift for the near-planar, near-confocal and near-concentric cavity configurations.

Results from Table 1.1 have as a consequence that the near-planar situation has the different transverse modes (l, m) associated to the same longitudinal q mode clustered on the high frequency side with respect to the fundamental Gaussian mode $(l, m) = (0, 0)$. The near-confocal situation has two cases, for transversal (l, m) modes with q fixed it depends on whether the sum $l + m$ is even or odd. In the even case the mode $(2, 0)$ or $(0, 2)$ is degenerate in frequency with the fundamental mode $(0, 0)$ but with $q + 1$, the modes which sum $l + m$ is 4 appear in the same frequency as the fundamental mode but with longitudinal order $q + 2$ and so on, the same happens for the odd case however now the modes are located halfway between the q longitudinal modes. Lastly for the near-concentric resonator the modes are clustered to the low frequency side of the fundamental mode, this because transverse modes (l, m) get displaced near the longitudinal fundamental mode $q' = q + l + m$. The above is illustrated in Figure 1.8.

1.3.2 Losses

In the above case only one frequency for each mode is resonant, this is an ideal case of a perfect cavity without losses. However there are different sources for optical losses: diffraction losses from the finite size of the mirrors, scattering losses in the mirror coatings, and transmission and absortion by the mirrors. Introducing them will broaden the spectral lines, meaning the lossy resonator can sustain waves within a vicinity of frequencies and not only a single frequency per mode.

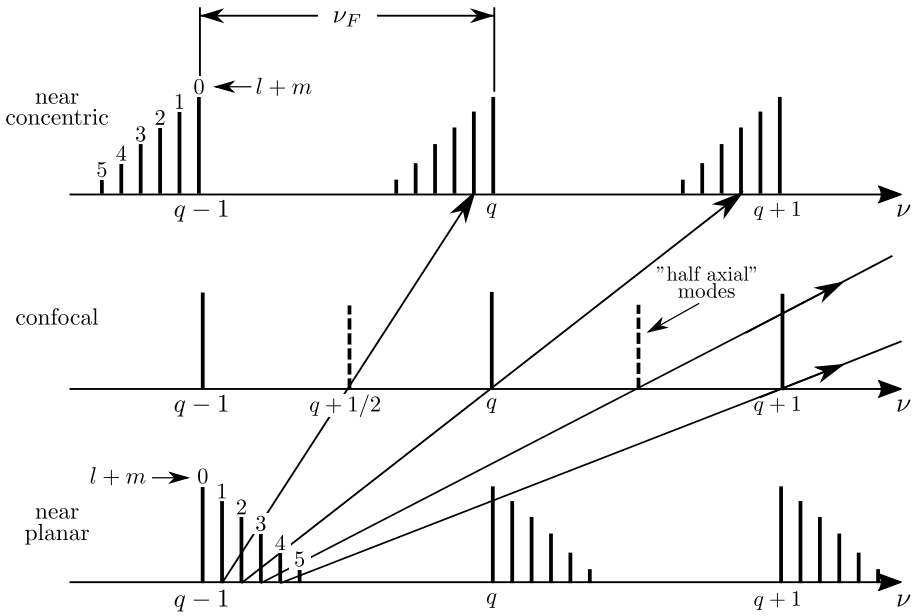

Figure 1.8: Resonant frequencies of transversal modes for different symmetric cavity configurations

To analyze how is the field inside the resonator we will assume the field changes by an attenuation factor $|r_a|$ multiplied by an acquired phase $e^{-j\phi}$ after each round trip. If the initial field is U_0, then after bouncing from the two mirrors it is $U_1 = hU_0$ where $h = |r_a|e^{-j\phi}$. In the end the field inside the cavity is the superposition of all this subsequently attenuated fields

$$U = U_0 + hU_0 + h^2U_0 + ... = \frac{U_0}{1-h}. \tag{1.26}$$

Using the trigonometric identity $\cos 2\theta = 1 - 2\sin^2\theta$ the intensity is in consequence

$$I = |U|^2 = \frac{|U_0|^2}{|1-|r_a|e^{-j\phi}|^2} = \frac{I_{max}}{1+(2\mathcal{F}/\pi)^2\sin^2\phi/2} \tag{1.27}$$

where $I_{max} = \frac{I_0}{(1-|r_a|)^2}$ and

$$\mathcal{F} = \frac{\pi\sqrt{|r_a|}}{1-|r_a|} \tag{1.28}$$

will be the finesse of the resonator. It is an important quantity to describe an optical resonator and is independent of its geometrical properties. Other definitions can be found in literature as described in [20] however for high mirror reflectivity all of them are coincident.

With respect to the attenuation factor $|r_a|$ two kinds of losses can be included as pointed by [18]. "Lumped losses" which occurr only at descrete locations, and "distributed losses" that take place within the medium of the cavity. The first ones corresponding to an intensity attenuation proportional to each mirror reflectance $R_1 = |r_1|^2$ and $R_2 = |r_2|^2$, and the second ones due to absortion and scattering within the medium between the mirrors. Its round trip attenuation factor is written as $e^{-2\alpha_s L}$, where α_s is the loss coefficient of the medium. Thus the total round-trip intensity attenuation factor is:

$$|r_a|^2 = R_1 R_2 e^{-2\alpha_s L}. \tag{1.29}$$

Equation (1.27) can be worked out substituting ϕ by the round trip acquired phase shift from equation (1.19), writing k in terms of frequency ν and using the definition of free spectral range to get the intensity as a function of frequency as:

$$I = |U|^2 = \frac{|U_0|^2}{|1 - |r_a|e^{-j\phi}|^2} = \frac{I_{max}}{1 + (2\mathcal{F}/\pi)^2 \sin^2\left[\pi\nu/\nu_F + (l + m + 1)\Delta\zeta\right]}. \tag{1.30}$$

This Airy distribution describing the intensity inside the cavity is plotted in Figure 1.9 for the fundamental Gaussian mode ($l = 0, m = 0$). The frequency spacing as it has been already seen corresponds to the free spectral range and the full width at half maximum when $\mathcal{F} >> 1$ turns out to be:

$$\delta\nu \approx \frac{\nu_F}{\mathcal{F}}. \tag{1.31}$$

The above equation shows that diminishig the finesse of the resonator broadens the transmision peak width and vice versa. From equations (1.28) and (1.29) it can be seen that the finesse diminishes when increasing the loss coefficient of the medium inside the cavity. For example, if we introduce a transparent medium with absortion and scattering like the windows of the vacuum chamber which houses the Rydberg atoms experiment mentioned in chapter 1, an additional loss should be multiplied in the total round-trip intensity attenuation factor in cosequence diminishing the finesse. The best option to increase finesse is by improving the mirrors reflectivity.

Reflection and Transmission

It is of interest to obtain a formula for the reflected and transmitted intensity spectra from the cavity, since this quantities can be directly measured and will have applications when it comes to lock the cavity length.

We examine how the electric field is affected by the cavity mirrors, first assume

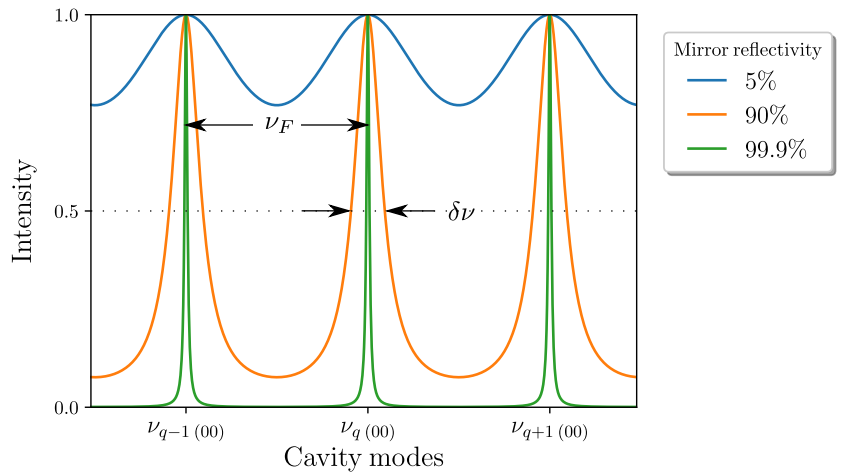

Figure 1.9: Spectra of a cavity with losses for the fundamental Gaussian mode at different mirror reflectivities.

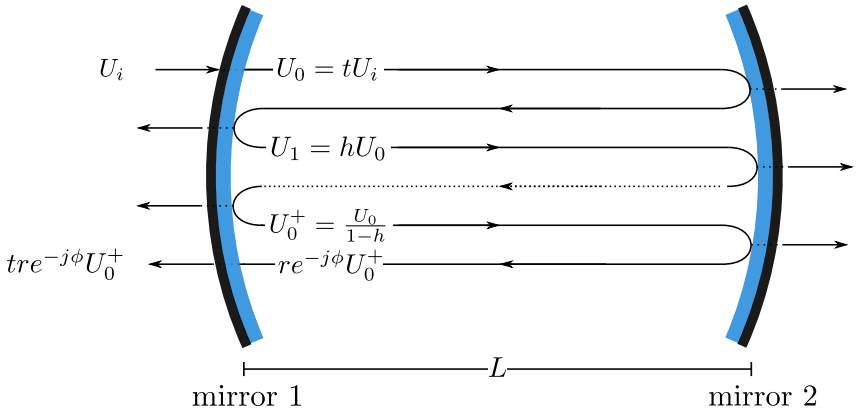

Figure 1.10: Schematic for the derivation of the cavity reflected field.

both mirrors have the same field transmission and reflection coefficients t and r. For convinience we will call U_0^+ to the total field inside the resonator which is already known from equation (1.26), assuming the incident field on the cavity is U_i then $U_0 = tU_i$ since U_0 was defined as the initial field inside the resonator, thus:

$$U_0^+ = \frac{tU_i}{1-h}. \tag{1.32}$$

and now $h = |r_a|e^{-j\phi} = r^2e^{-j\phi}$ where ϕ was the round-trip acquired phase and r^2 comes from the reflection at the two mirrors. To obtain the total reflected field U_r from the cavity it is necessary to reflect U_0^+ from the second mirror, add the acquired phase $e^{-j\phi}$ and then transmit from the first mirror. Also the reflected incident field rU_i needs to be added. Figure 4.1 shows a schematic of this, then

$$U_r = -rU_i + \frac{t^2 r e^{-i\phi} U_i}{1 - r^2 e^{-i\phi}}. \tag{1.33}$$

Simplifying this equation and noting that the acquired round trip phase is $\phi = 2kL = 2\pi\nu/\nu_{FSR}$ the reflection coefficient of the cavity is found to be

$$\mathcal{R}(\nu) = \frac{U_r}{U_i} = \frac{r\left(e^{2\pi\nu/\nu_{FSR}} - 1\right)}{1 - r^2 e^{2\pi\nu/\nu_{FSR}}}. \tag{1.34}$$

In a similar fashion the transmission coefficient can be derived and written as:

$$\mathcal{T}(\nu) = \frac{U_t}{U_i} = \frac{(1 - r^2)\, e^{2\pi\nu/\nu_{FSR}}}{1 - r^2 e^{2\pi\nu/\nu_{FSR}}}. \tag{1.35}$$

The above equations for reflection and transmission coefficients can easily be transformed into functions of cavity length noting that $\nu/\nu_{FSR} = 2L/\lambda$ this means the cavity modes are appart integer multiples of the free spectral range or half of the wavelength.

This Airy distributions are the most common approach to model the spectrum of a symmetric resonator with losses, however as pointed in [21] each resonant peak has a Lorentzian line shape of the form:

$$\mathcal{T}(\nu) = \frac{T_0}{4(\nu - \nu_q)^2/\delta\nu_q^2 + 1}, \tag{1.36}$$

where T_0 is a transmission coefficient, ν_q is a resonant frequency and $\delta\nu_q$ is the linewidth of the cavity mode. This expression can be obtained when expanding the sine function of equation (1.30) to second order around a resonant frequency ν_q. Thus the above Airy distributions come from summing up individual mode profiles with Lorentzian distributions.

Chapter 2

Near Concentric Cavity Prototype

In this work we focus on building a prototype for the cavity. Our main interest is to explore how near the concentric regime can we get. For this reason we plan a resonator considering how small can we get the waist and a method to tune the resonator length.

2.1 Mirrors

The cavity waist should be small enough to allow only one Rydberg blockade sphere within the atomic cloud, this means for Rydberg states with principal quantum number between 80 and 100 we would desire the waist to be of about 5 µm. This is a very small waist, if we were to build a confocal cavity, which is the most stable one, the distance between mirrors should be of about 0.2 mm and the mirrors would also have a very small radius of curvature. For this reason it is necessary to plan a near-concentric cavity which allows a small waist with greater radius of curvature for the mirrors and cavity length.

The first parameters we fix are the radius of curvature for the mirrors. The available space inside the vacuum chamber for the cavity limits the cavity length to a maximum of 15 cm, so we impose it to be of 10 cm thinking on the space the mirror mounts and cavity structure will need inside the vacuum chamber. Using the desired length, waist and considering light of 780 nm we calculate the appropiate radius for the mirrors using equation (1.13d) yielding approximately 5 cm.

Decreasing the radius of curvature implies a reduction to the cavity length since in the near-concentric regime $L \approx 2R$ and as a consequence the mode volume decreases improving the atom-cavity coupling strength and the minimum achievable waist. The problem of getting the mirrors to close is losing optical access for the magneto-optical trap (MOT) beams, contamination of cavity mirrors by the atomic sample, the need for mirrors with small radius of curvature and the fact that deposited charges in the mirrors would affect the atoms transition frequencies because Rydberg atoms are quite sensitive to electric fields. Considering this, we use a pair of dielectric-coated concave mirrors with a radius of curvature of 5 cm and 12.7 mm of diameter from Thorlabs with part number CM127P-025-E03. This mirrors are constructed to have a mirror reflectance greater than 99% and an absorption lower than 1% from 750 nm to 1100 nm. Meaning the finesse of the cavity will be of at least 312 according to equation (1.28).

Now using the condition of equation (1.19) for the acquired phase to be a multiple of 2π. We derive an equation dependent of the cavity length L and the longitudinal index q which is

$$kL - 2\arctan\left(\sqrt{\frac{L}{2R-L}}\right) - \pi q = 0. \tag{2.1}$$

This equation is solved numerically to get a list of the last possible length resonant values considering their discrete character given by their longitudinal q index. For convinience we express the length in terms of the distance from the concentric regime as $\Delta L = L_{concentric} - L$ and we call this the critical distance. Using the already chosen parameter for the radius of curvature of the mirrors we calculate the waist and plot the possible resonant modes before the concentric regime in Figure 2.1. This plot confirms the possibility of achieving waists near 5 µm.

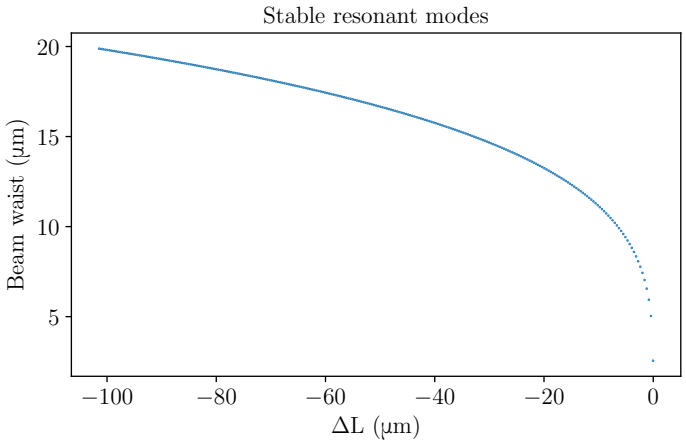

Figure 2.1: Waist versus mirror distance near the concentric regime. Calculated for a cavity with $R = 5$ cm and 780 nm as wavelength.

However it is necessary to take into account how much does the waist scales at the mirrors when the cavity approaches the concentric regime because theoretically in this limit the waist becomes infinite at the mirrors. Figure 2.2 shows how the beam achieves waists from 5 mm to less than 1 mm when the length moves away from the concentric regime. This is an important detail to consider since the mirrors diameter must be at least 4 times the beam waist to reflect the 99.97% of the beam power and in consequence minimize diffraction losses and allow the injection of the complete matched mode to the cavity without exciting higher order modes. In our case considering an effective aperture of 12 mm for our mirrors we could expect to have a beam with a maximimum waist at the mirrors of 3 mm.

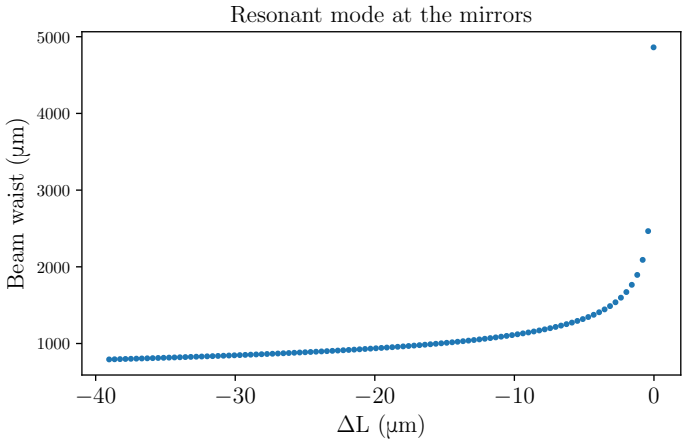

Figure 2.2: Waist at the mirrors when approaching the concentric regime. Calculated for a cavity with $R = 5$ cm and 780 nm as wavelength.

2.2 Displacement

As Figure 2.1 shows and was explained in the theory, longitudinal modes are separated by a distance equal to half a wavelength. In order to mantain the cavity alignement it is needed a fine tuning of its length with a precision within hundreds of nanometers. Mechanical vibrations and thermal expansion can easily move appart the mirrors considerably in this scales. For this reason it is necessary to control precisely the distance between mirrors, as a solution a piezo electric is mounted to move one of the mirrors longitudinally. The piezo is from Thorlabs with part number TA0505D024W, was selected because it can displace 2.8 μm ± 15% and this is enough distance to cover more than a free spectral range and compensate for thermal drifts.

2.3 The Design

The plan is to know from our prototype what aspects we need to take into account when designing a mount for the cavity which can be placed inside vacuum. The important aspects are what do we need to achieve the mode matching, how important is it to tune each mirror tilt and how can we effectively achieve the longitudinal displacement for one of the cavity mirrors.

To find a solution for this queries we propose to build a simple prototype mounting the mirrors on kinematic mirror mounts with height fixed but with angular adjustment available. One of the mirror mounts is placed above a Thorlabs translational linear stage with a side mounted micrometer (XR50P). The piezo is placed between the micrometer tip and the translational stage allowing the longitudinal displacement. This configuration is depicted in Figure 2.3.

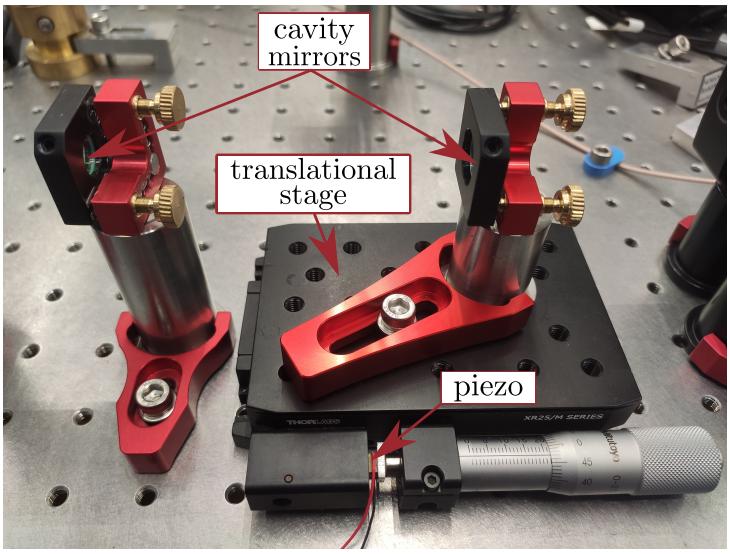

Figure 2.3: Photo of the cavity prototype. Both mirrors are placed on rotational kinematic mounts with fixed height. A translational stage with an incorporated piezo allows cavity length scanning and tuning.

The optical array which allows mode matching, cavity alignement and monitoring of reflection and transmission is as shown in Figure 2.4. Light is obtained from a polarization-maintaining single-mode fiber, polarization axis of light is defined by a $\lambda/2$ plate and a polarization beam splitter (PBS), then light goes through a mode-matching lens system and finally to the cavity. The reflection is separated by a $\lambda/4$ plate and the PBS and examined through a Thorlabs (DET36A2) photodiode. Transmission is monitored with a CCD camera which can also be replaced by a photodiode.

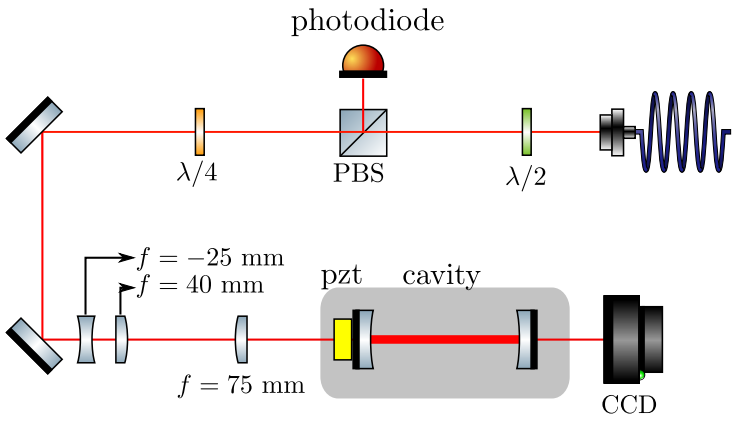

Figure 2.4: Optical array for the resonator. This array allows to scan the resonator length and monitor the cavity reflection and transmission.

Lens focal length	Manufacturer	Part number
−25 mm	Thorlabs	$LD2297 - B$
40 mm	Thorlabs	$LA1422 - B$
75 mm	Thorlabs	$LA1608 - B$

Table 2.1: Mode-matching lens system components.

2.4 Alignment Process

Alignment is a delicate matter as mentioned by Anderson [22] a bad coupling of the light to the cavity excites higher order spatial eigenmodes rather than the fundamental gaussian mode.

Mode Matching

Before aligning the mode matching lenses should be selected so the correct sized gaussian mode is injected into the cavity. The beam comes from an optical fiber and is then collimated by an $f = 11\,\text{mm}$ lens, a measurement of the beam waist yields $(0.87 \pm 0.03)\,\text{mm}$. As it can be seen from Figure 2.2 the mode in the near concentric regime acquires a large waist at the mirrors, so we first expand and collimate the beam with a Galilean telescope. After that convergent lens focuses the beam to the cavity center. Mode matching optics were selected so the beam could be completely contained within our lenses of one inch diameter. For the Galilean telescope the lenses where $f = -25\,\text{mm}$ and $f = 40\,\text{mm}$, and the focusing lens has a focal distance $f = 75\,\text{mm}$. This system would theoretically yield a $25\,\mu\text{m}$ waist at the center of the cavity.

Alignment

We start by defining the optical axis with a lot of care by pointing the laser beam at 75 mm of height parallel to the optical table. After that the mode matching lenses are introduced taking care of not moving the optical axis. Then the furthest cavity mirror

(second mirror) is introduced and its reflection is carefully aligned to point in the same path as the incident beam. Finally the first cavity mirror is introduced and aligned with help of the CCD camera while the laser is scanning its frequency. This camera shows the transmission from the cavity and the mirror is fixed when low order transmitted modes start to appear. In the above process it is important to take care the beam points at the center of the mirrors to minimize diffraction losses and obtain a better coupling.

Mode coupling is then refined by movements of the mirror tilt starting with the first mirror and compensating with the second mirror. The objective here is to minimize the order (size) of the coupled modes to arrive to the fundamental gaussian mode. When this is done, the reflected Airy characteristic spectra is monitored with a photodiode and alignment is further refined by adjusting the two mirrors that couple light to the cavity. It is easier first to align the cavity when it is some distance apart from concentric and after that move gradually the second mirror with a translation stage until a near concentric regime is obtained.

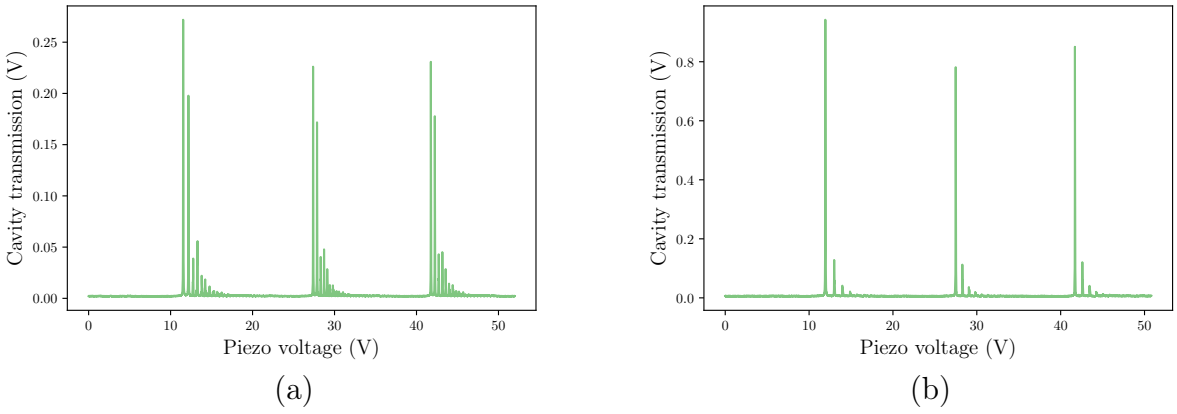

Figure 2.5: a) Before improving alignment higher order modes are coupled to the cavity. b) After alignment higher order modes coupling is considerably reduced.

2.5 Misalignment Losses

The ideal cavity is that in which mirror tilt and optical axis are perfectly aligned. Misalignments can be classified in terms of a bad mode matching when the cavity theoretical waist is not in accordance with the injected mode waist size or longitudinal position, this situation excites Laguerre-Gaussian modes in the cavity. Or in terms of a bad optical axis matching, the beam might be parallel off-axis or it might be tilted with respect to the optical axis causing excitation of higher order Hermite-Gaussian modes[22]. Correct alignment means the fundamental mode is perfectly coupled to the cavity maximizing the ratio of power coupled to the fundamental mode to power injected.

To better analize diffraction loss due to mirror tilt, remember the mode was planned to have a maximum waist at the mirrors of 3 mm which corresponds to one fourth of the

mirrors effective aperture and a reflection of 99.97% of the beam power. As a matter of fact this is not enough to avoid diffraction ripples since an effective aperture of $4.6w_0$ still causes 1% of intensity variation with respect to total intensity[19], so the mode will have this distortion due to this finite aperture effect.

Another important aspect is how much a mirror tilt α causes an inclination of the optical axis. A general formula for this can be consulted in [23], however for our purposes we consider a simplification for symmetric cavities. As illustrated in Figure 2.6, consider one mirror is tilted by an angle α with respect to its perfect aligned position. In consequence the optical axis (OA) changes its position acquiring an inclination θ. Assuming α is small ($\sin\alpha \approx \alpha$) geometrically it follows that:

$$\tan\theta = \frac{R\alpha}{2R - L} = \frac{\alpha}{1+g}. \tag{2.2}$$

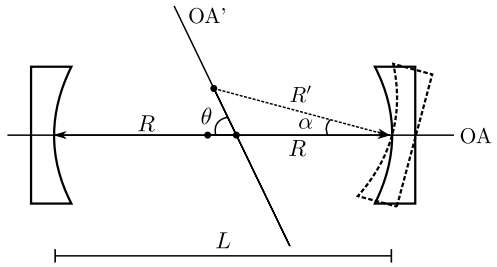

Figure 2.6: In the near concentric regime a small mirror tilt α causes a great change in the optical axis (OA).

The last equation for a near concentric configuration ($g \to -1$) shows how a small tilt of one mirror is enough to rotate almost 90° the optical axis, it means alignment becomes harder since the optical axis easily moves away from the finite mirrors surface. This situation is different for the confocal or near planar configurations as shown in Figure 2.7.

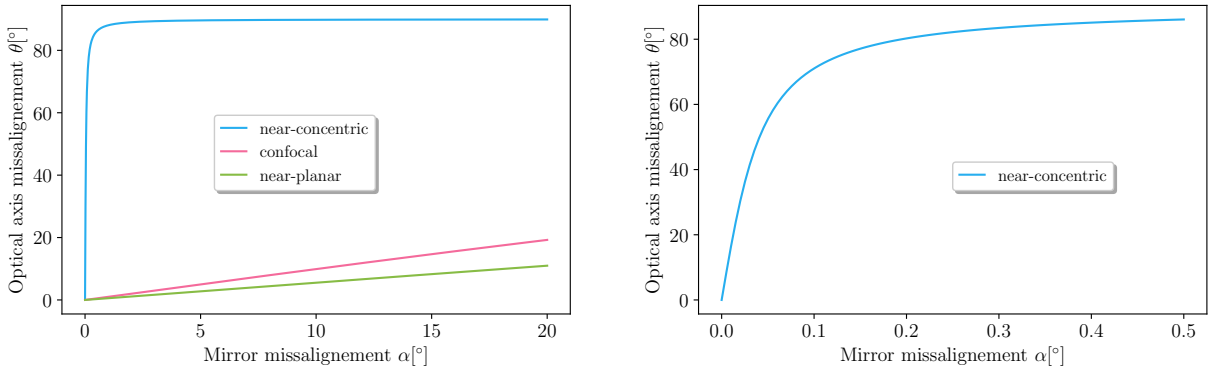

Figure 2.7: In the near-concentric limit the optical axis tilts considerably more than in the confocal or near-planar configurations with respect to a mirror tilt. a) Plot of equation (2.2), for the near concentric situation with parameters $R = 5$ cm and length $L = 99.97$ mm, the confocal situation $R = L = 5$ cm and near planar situation $R = 5$ cm and $L = 10$ mm. b) Detail for the near-concentric configuration for small mirror tilts.

Chapter 3

Cavity Characterization

This chapter describes the parameters of the cavity which can be measured to characterize it.

3.1 Hermite and Laguerre-Gauss Modes

After alignment of the cavity the transmission signal is recorded as shown in Figure 3.1. Coupling to higher order modes is still observed, this can be corrected by means of adjusting the mode matching lenses and adjusting the coupling mirrors. As mentioned by Anderson [22], Hermite-Gauss modes get coupled because of a translation or tilt of the incident beam with respect to the optical axis defined by the mirrors and Laguerre-Gauss modes can be observed when the mode is mismatched by an incorrect waist beam size or position.

3.2 Length Measurement

Measuring the distance between mirrors is achieved by means of the cavity free spectral range (equation (1.23)). We use two narrow linewidth lasers of 780 nm, the first locked to an ultra stable high finesse cavity using the Pound Drever Hall technique (PDH) (section 4.1.1) and the second locked with respect to the first one by a frequency beat. This

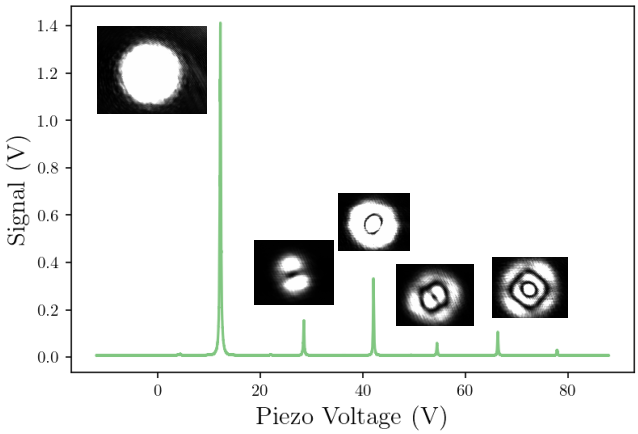

Figure 3.1: Transmission spectra of the cavity while scanning with the piezo. Optical axis or mode-matching misalignment causes excitation of higher order modes apart from the fundamental.

technique allows us to know precisely the relative frequency between both lasers. We send them through the cavity while its length is being varied by the piezo and record the transmission using a photodiode. As it is shown in Figure 3.2 the transmission shows a peak when the fundamental mode is coupled for each laser, after that we move the relative frequency between them. This makes the peaks to overlap, which means the lasers are apart a frequency equal to an integer multiple of the free-spectral range.

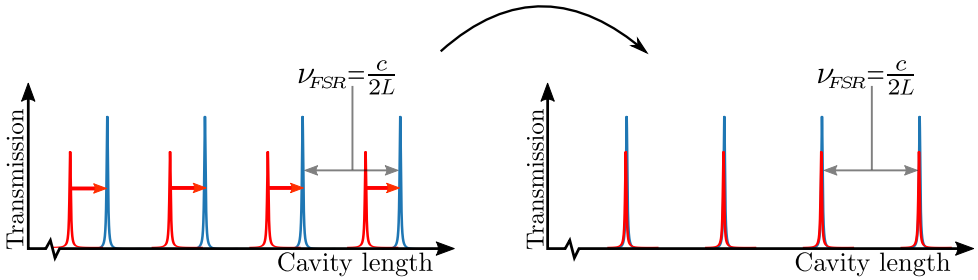

Figure 3.2: Left plot shows transmission of the fundamental mode by two lasers with different frequency while varying cavity length. One laser depicted in blue and the other in red. Right plot represents when the frequency between both lasers equals a free spectral range or an integer multiple of it, the two peaks overlap.

To make a quantitative measurement of the frequency where both lasers fundamental mode peaks overlap, we record the position of both peaks as a function of detuning between the lasers. We take care that the range of detunings used ensures that the peak that moves completely crosses over the other one from side to side. As shown in Figure 3.3 from a) to d) a Lorentzian function is fitted to both peaks and from that the distance between centers is calculated as the relative frequency between lasers is changed. After that an interpolation is made by fitting a line to calculate the frequency for which the lorentzian peaks will be perfectly overlapped as shown in Figure 3.3 e). This interpolation is needed to improve precision because the width of each peak makes unclear the exact frequency for which both peaks overlap. The error we report from this interpolation method comes from the standard deviation associated to the intercept constant of the linear fit.

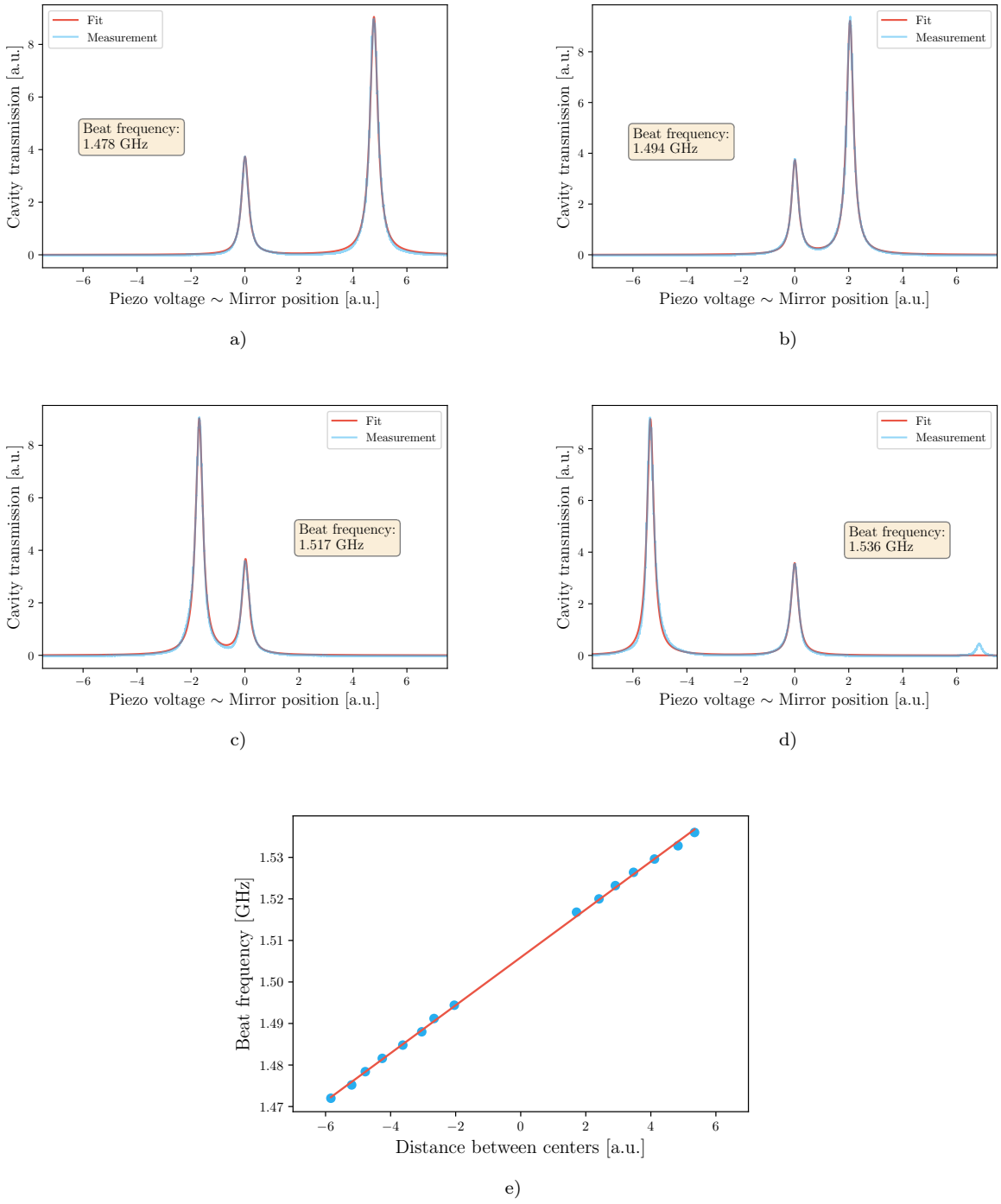

Figure 3.3: a) to d) show how the fundamental mode transmission peaks of two lasers with different frequency approach as the relative frequency between them approaches the free spectral range as recorded directly from the oscilloscope. The minor peak comes from the transmission of a frequency fixed laser and the other peak moves when varying the frequency of its respective laser. Horizontal axis is proportional to the voltage ramp applied to the piezo which in turn is proportional to the mirror position. Vertical axis is proportional to the voltage as recorded by the photodiode. e) corresponds to the distance between both peak centers as the relative frequency between lasers is varied. In this particular measurement the intercept frequency which is the free spectral range resulted 1505.9 ± 0.2 MHz corresponding to 99.54 ± 0.01 mm of distance between mirrors.

3.3 Gouy Phase

Measuring the Gouy phase will be useful to determine the beam waist as mentioned in [24]. Beam waist at the center of the cavity might be obtained using only the free spectral range by means of equation (1.13d) however the formula is dependent on the radii of curvature of the mirrors which adds uncertainty, also requires approximating the cavity to be cylindrically symmetric and one must trust in the manufacturer precision. Alternatively, we can measure the free spectral range and the separation between transverse modes to measure the beam waist via the Gouy phase without making assumptions about the mirrors' radii of curvature.

As pointed in [25] the best approach to gain access to the Gouy phase is by means of the higher order transverse modes of the cavity. This is because equation (1.22) implies that

$$\Delta\zeta = \frac{\pi(\nu_{l,m,q} - \nu_{l',m',q})}{[(l+m) - (l'+m')]\nu_F}. \tag{3.1}$$

From the latter, the resonator g-parameters can be obtained by equation (1.25) and in consequence a substitution on equation (1.13d) provides a value for the cavity beam waist. It is only needed to identify the free spectral range and the distance between higher order modes.

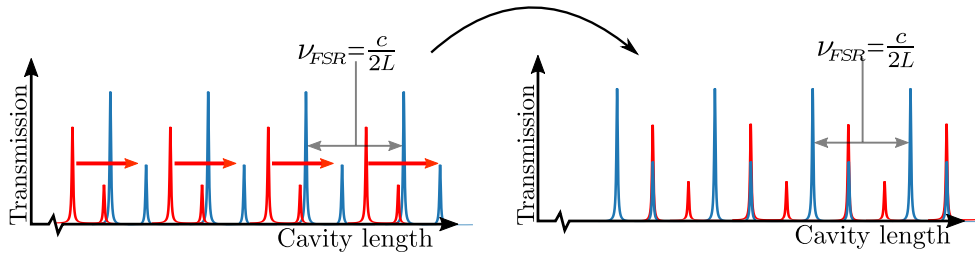

Figure 3.4: When cavity is slightly misaligned the first order Hermite-Gaussian (HG) mode appears besides the fundamental Gaussian mode. Left plot shows transmission of the fundamental mode and first order HG mode by two lasers with different frequency while varying cavity length. One laser depicted in blue and the other in red. Right plot represents when the frequency difference between both lasers equals the distance from the fundamental to the first order HG mode or an integer multiple of it, the fundamental peak of one laser overlaps the first order HG mode of the other laser.

The measurement of the distance between higher order modes is carried out by the same procedure mentioned before in the case of the free-spectral range determined by the detuning between two frequency-stabilized lasers.

We started measuring the free spectral range and distance between the fundamental and first order Hermite-Gaussian mode of the cavity in an arbitrary position near concentric. From this data cavity length and waist can be calculated as it has already been explained.

The initial distance turned out to be (97.440 ± 0.008) mm from this point we moved the micrometric stage by steps, realigned and measured until the furthest possible near concentric mode was achieved. This point corresponded to a distance between mirrors of (99.944 ± 0.008) mm and a waist of (19.3 ± 0.4) μm). At this position the cavity mirrors where highly sensitive and adjustment required more precise kinematic mirror mounts, making almost impossible further alignment into a more near concentric regime, also cavity transmission was quite unstable due to any ambient noise and mode coupling started to reduce causing error to rise when approaching concentric configuration. This results can be seen in Figure 3.5. From each distance and Gouy phase measurement, the mirrors' radius of curvature can be calculated, averaging the results obtained from each step we moved the cavity length gives an experimental measurement of 5.002 ± 0.005 cm, which is in agreement with the manufacturer specifications of 5 cm.

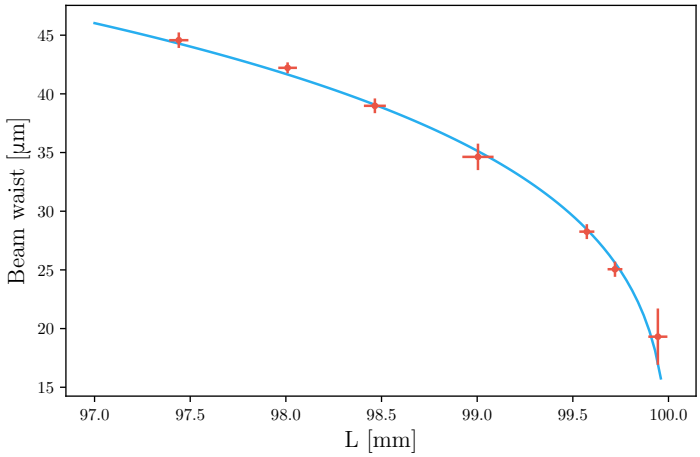

Figure 3.5: Waists measured from the spectral separation of Hermite-Gaussian modes and free spectral range versus distances obtained directly from the free spectral range measurements when varying cavity length.

3.4 Finesse

As it has been already pointed out mirrors specifications establish a lower bound of 312 for the finesse. To measure it we capture the transmission of the fundamental mode by the cavity when scanning the piezo, fit a lorentzian function and determine its width. To calibrate the frequency scale we generate sidebands by means of an electro-optic modulator (EOM) at 12.5 MHz to use as a reference. This can be seen in Figure 3.6.

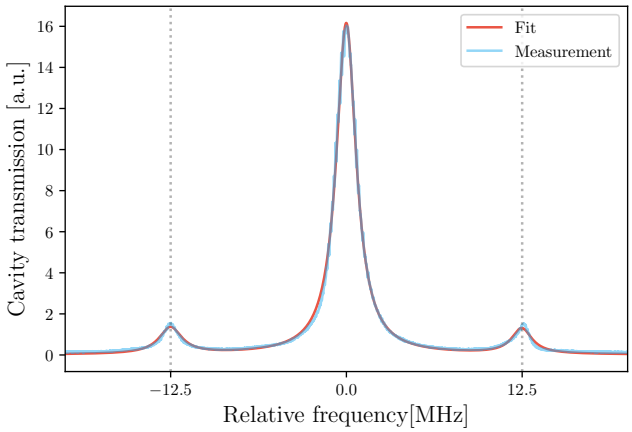

Figure 3.6: Transmission spectra of the cavity while scanning with the piezo. Optical axis or mode-matching misalignment causes excitation of higher order modes apart from the fundamental.

The measured width corresponds to $1.96 \pm 0.02\,\text{MHz}$ which combined with the free spectral range of $(1499.8 \pm 0.1)\,\text{MHz}$ measured in the previous section for the furthest near concentric resonant mode achieved gives a finesse of 765 ± 8, when using the formula 1.31. It means the mirror's reflectivity must be higher than 99%, at least they have a lower bound of 99.6%. This is because mirror reflectivity might be higher but there might be other losses which also diminish the finesse as explained in section 1.3.

Chapter 4

Cavity Stabilization

Stabilization is crucial for maintaining the cavity at resonance. Considering that a length variation in the order of half a wavelength is enough to change the fundamental longitudinal mode to its adjacent fundamental mode a very precise way to move the cavity mirrors must be used. Moreover, from the previous chapter we know the resonance peak width is approximately 2 MHz, the free spectral range 1500 MHz and the wavelength 780 nm, using the relation $\nu/\nu_{FSR} = 2L/\lambda$ from section 1.3, we can estimate the cavity is resonant within 0.5 nm of mirror displacement. For this reason, cavities are usually stabilized in temperature to avoid thermal drift using materials with low expansion coefficients such as Invar, carbon fiber, rods of quartz or steel alloys with very low or zero expansion coefficients. Another option is to actively stabilize the length moving the mirrors to compensate thermal drift.

Active stabilization also protects the cavity against mechanical vibrations and acoustic noise which affects its length altering its spectrum. The solution to actively stabilize the length is moving the mirrors fast enough to compensate all possible perturbations.

4.1 Cavity Lock

Locking the system refers fixing the cavity length in a resonance peak of its spectra relative to a frequency stabilized laser. For this we use the Pound Drever Hall (PDH) technique. This technique is a very powerful and popular method for stabilizing laser systems using a

high-finesse Fabry Perot cavity as a frequency reference [26–28]. It is commonly used in the field of gravitational wave detectors and atomic physics when a great frequency precision and low spectral width is required. In this work we use the Pound Drever Hall method in a different way, the laser is already stabilized in frequency and we aim to stabilize the cavity length.

To lock the cavity length we need a control system. In this case we use a proportional-integral-derivative controller (PID), this is an electronic feedback mechanism which compares a continuously measured variable, for example temperature, speed, intensity, etc., with a desired setpoint and applies a correction based on the difference that exists between the measured variable and its desired value. This difference is called the error, and the correction used to minimize the error is based on proportional, integral and derivative terms obtained from this error. Thus a PID is capable of keeping a variable at a desired setpoint, in other words it keeps the error near zero. For the cavity we would like to keep it at resonance with the incoming light thus we need a method to calculate the error using as setpoint the resonance peak maximum. However there is a problem because of the peak's symmetry, if the cavity length moves around this resonance the resulting error is the same to the right and to the left of the transmission peak, thus the controller can not notice the difference between diminishing or increasing cavity length. The Pound Drever-Hall technique provides a method to generate an asymmetrical signal around the transmission peak's maximum to make possible for the controller to apply a correction.

4.1.1 Pound-Drever-Hall (PDH) Technique

The problem that this method solves is how to actively keep constant the frequency of a laser, or in our case the length of the cavity, with respect to a stable reference usually an ultra-stable cavity, or in our case an stabilized laser. PDH technique generates an error signal to tell a control system how to keep a system stable [26]. The following analysis of how to produce PDH error signal is the same in the case of moving the laser frequency or the cavity length since the spectra of the resonator is the same in both cases.

Lets start by considering the reflected signal while varying the length of the resonator given by equation (1.34) and illustrated in Figure 4.1, this turns out to be better than the transmission since the peaks depth is less sensitive to the light intensity variation. If we were to tell a PID to fix the length in the tip of a reflection peak there would be a problem since moving the length around the peak gives no information of whether the length should be increased or decreased. An effective way to overcome this issue is to feed the derivative of the reflected signal to the control system. To the left from the tip of the peak the derivative is an increasing negative function and to the right it is increasing positive, with this information the control system will be capable of increasing or decreasing the cavity length depending on the sign of the derivative in order to stay at the zero value of the derivative which means it will stay at the tip of the peak.

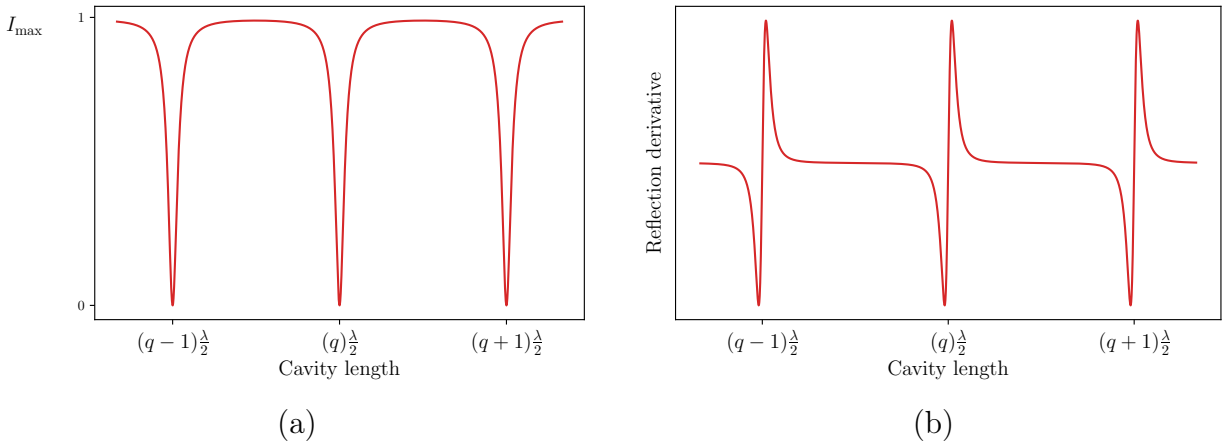

Figure 4.1: a) Resonator reflection when varying cavity length. b) Resonator reflection derivative when varying cavity length.

Conveniently this derivative is not hard to get, varying sinusoidally the frequency of the laser will create a variation in the reflection, to the right of the peak this variation causes the reflected intensity to vary proportional, i.e. in phase, with the laser frequency modulation. Conversely to the left of the tip this variation goes inversely proportional, i.e. out of phase by 180°, as shown in Figure 4.2. Then we need to make a phase sensitive measurement, to get the relative phase of the reflected intensity with respect to the modulation signal that drives the laser frequency.

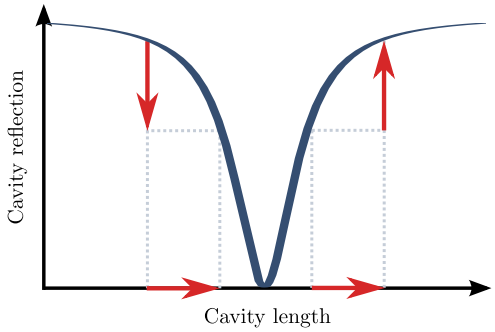

Figure 4.2: Reflected intensity while varying cavity length. To the right of the peak a length increment causes an intensity gain and to the left this increment causes intensity loss.

To understand how this measurement is done, we need to make a quantitative analysis. We start by writing the field d of the phase modulated laser beam incident on the cavity as

$$E_i = E_0 e^{i(\omega t + \beta \sin \Omega t)}, \tag{4.1}$$

where ω is the original beam angular frequency, Ω is the phase modulation frequency, and β is known as the modulation depth. This expression can be expanded in terms of Bessel functions using the Jacobi-Anger expansion, to

$$\begin{aligned} E_i &\approx \left[J_0(\beta) + 2iJ_1(\beta)\sin\Omega t\right] e^{i\omega t} \\ &= E_0\left[J_0(\beta)e^{i\omega t} + J_1(\beta)e^{i(\omega+\Omega)t} - J_1(\beta)e^{i(\omega-\Omega)t}\right]. \end{aligned} \tag{4.2}$$

This means the field now has the original angular frequency ω plus two sidebands centered at $\omega \pm \Omega$. Then using equation (1.34) and summing individually for each frequency component we calculate the reflection from the cavity using this incident field to be

$$E_r = E_0\left[\mathcal{R}(\omega)J_0(\beta)e^{i\omega t} + \mathcal{R}(\omega+\Omega)J_1(\beta)e^{i(\omega+\Omega)t} - \mathcal{R}(\omega-\Omega)J_1(\beta)e^{i(\omega-\Omega)t}\right]. \tag{4.3}$$

In consequence the power of the reflected beam $P_r = |E_r|^2 A$, which is measured by the photodetector of area A, is

$$\begin{aligned} P = |E_r|^2 = P_c|\mathcal{R}(\omega)|^2 &+ P_s\left\{|\mathcal{R}(\omega+\Omega)|^2 + |\mathcal{R}(\omega-\Omega)|^2\right\} \\ &+ 2\sqrt{P_cP_s}\,\mathrm{Re}\left[\mathcal{R}(\omega)\mathcal{R}^*(\omega+\Omega) - \mathcal{R}^*(\omega)\mathcal{R}(\omega-\Omega)\right]\cos\Omega t \\ &+ 2\sqrt{P_cP_s}\,\mathrm{Im}\left[\mathcal{R}(\omega)\mathcal{R}^*(\omega+\Omega) - \mathcal{R}^*(\omega)\mathcal{R}(\omega-\Omega)\right]\sin\Omega t \\ &+ (2\Omega \text{ terms}). \end{aligned} \tag{4.4}$$

This equation has the corresponding power of the three individual frequencies, terms who oscillate with Ω that correspond to the interference between the carrier and the sidebands and 2Ω terms which correspond to the interference between the sidebands. We are interested in the sine or the cosine term, because as will be shown they sample the phase of the reflected carrier.

Error Signal

There are two regimes to analyze the reflected signal. When $\Omega \ll \Delta\nu_{FSR}\mathcal{F}$ (slow modulation) it turns out $\mathcal{R}(\omega)\mathcal{R}^*(\omega+\Omega) - \mathcal{R}^*(\omega)\mathcal{R}(\omega-\Omega)$ is purely real and in the opposite situation $\Omega \gg \Delta\nu_{FSR}\mathcal{F}$ (fast modulation) it results the term is purely imaginary. The second case gives a better error signal and is the standard used in PDH. In this situation the modulation frequency is high enough that the sidebands can not be resonant in the cavity at the same time as the carrier frequency. So the sidebands are totally reflected when the carrier frequency is resonant, this means $\mathcal{R}(\omega \pm \Omega) \approx -1$ in consequence

$$\mathcal{R}(\omega)\mathcal{R}^*(\omega+\Omega) - \mathcal{R}^*(\omega)\mathcal{R}(\omega-\Omega) \approx -2i\,\mathrm{Im}\left\{\mathcal{R}(\omega)\right\}. \tag{4.5}$$

Because of this in equation (4.4) the $\cos\Omega t$ term cancels out. And the remaining term

which oscillates as $\sin \Omega t$ will be

$$\epsilon = -2\sqrt{P_c P_s}\mathrm{Im}\left\{\mathcal{R}(\omega)\mathcal{R}^*(\omega+\Omega) - \mathcal{R}^*(\omega)\mathcal{R}(\omega-\Omega)\right\}, \tag{4.6}$$

which is plotted in Figure 4.3. This is a very convenient error signal since its asymmetrical with respect to the resonance length and is quite width around the resonance peak, so the control system can easily tune the length to lock it.

Considering the above discussion, equation (4.4) can be approximately written as:

$$P_{ref} \approx 2P_s - 4\sqrt{P_c P_s}\,\mathrm{Im}\{\mathcal{R}(\omega)\}\sin\Omega t + (2\Omega \text{ terms}). \tag{4.7}$$

The remaining problem is to isolate the central term of this equation, this is achieved using a frequency mixer and a low pass filter. When both inputs in a mixer are sinusoidal signals the resulting signal is their product which yields

$$A\sin(\Omega t)\, A'\sin(\Omega' t) = \frac{AA'}{2}\left\{\cos\left[(\Omega-\Omega')\,t\right] - \cos\left[(\Omega+\Omega')\,t\right]\right\}, \tag{4.8}$$

this equation shows that using $\Omega' = \Omega$ will make the $\cos(\Omega - \Omega')t$ a constant signal which can be isolated with a low pass filter and it is multiplied by the term (4.6) which is the error signal we need to feed the control system.

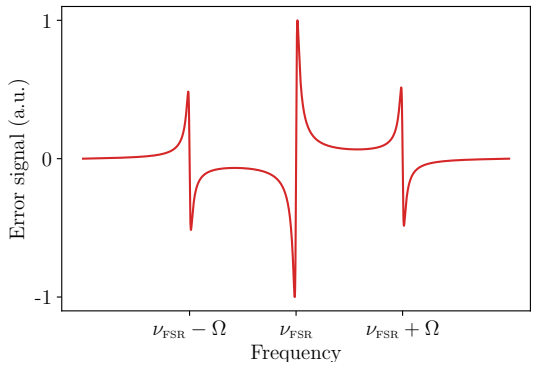

Figure 4.3: Theoretical Pound Drever Hall error signal for fast modulation.

Thus multiplying the reflected power using the frequency mixer with a sinusoidal function and passing the result through a low pass filter (to cut frequencies above Ω') isolates the error signal. The remaining issue is to equal the phase between the sinusoidal function with Ω and the one with Ω' so equation (4.8) remains valid, this is achieved using a phase shifter to adjust the phase of the Ω' oscillating term. A diagram for the PDH used arrangement is shown in Figure 4.4. Also measurements from the reflected signal with

modulation and PDH obtained error are shown in Figure 4.5.

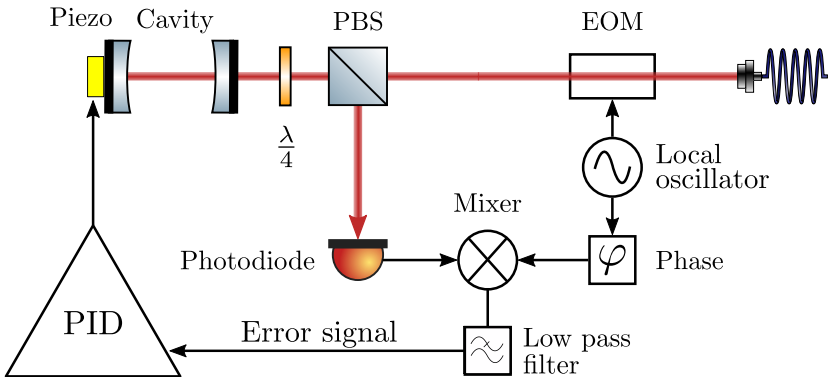

Figure 4.4: Setup for PDH method. The local oscillator is a function generator RIGOL DG1022Z of two channels, both are set to the same frequency and their relative phase is varied. A frequency of 12.5 MHz is fed to an EOM from Photonics Technologies (01-12.5-V-0159) and to the mixer ZP-1LH-S+ from Minicircuits, the low pass filter is from Minicircuits with part number SLP-5+. The photodiode to monitor cavity reflectance is DET36A2 from Thorlabs.

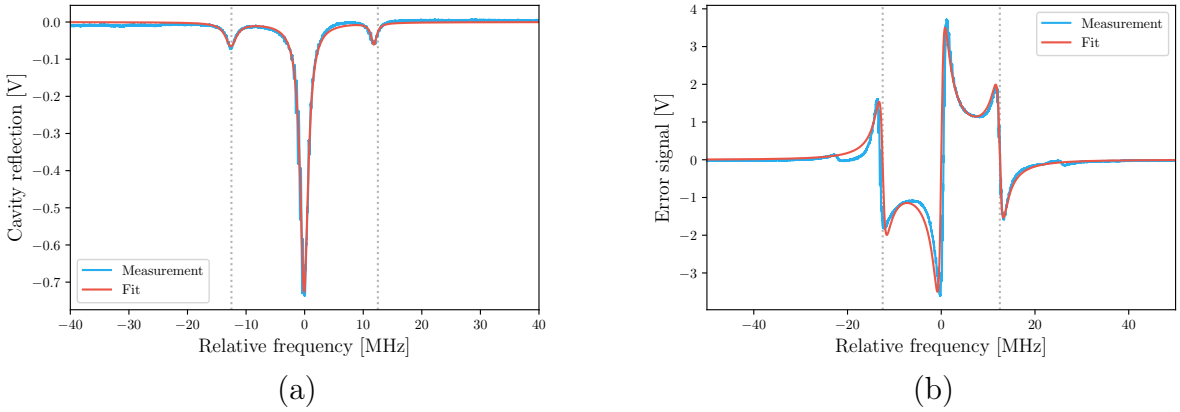

Figure 4.5: a) The fundamental gaussian mode peak with sidebands generated at 12.5 MHz. b)Pound Drever Hall error signal obtained from the reflected spectra with sidebands.

To lock the cavity length a homebuilt PID was used to feedback the cavity piezo given the error signal of Figure 4.5. It is possible to effectively lock the system oscillating around the fundamental peak, however in our current setup it is still necessary to improve the cavity design to get a faster response from the piezo since the control signal is dephased from the error signal. This slow response from the cavity makes the control system notice the change in the cavity length too late after a variation in the control signal is made. Causing the system to oscillate around the locking point as shown in Figure 4.6.

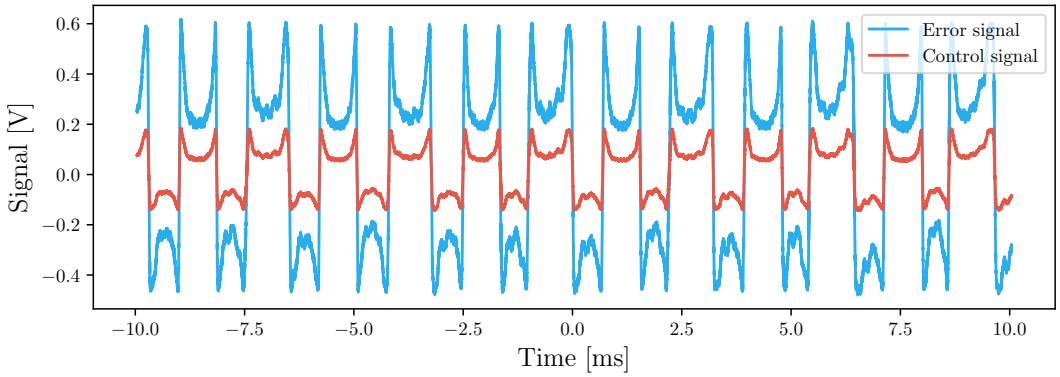

Figure 4.6: Blue signal corresponds to the error signal that is fed to the control system. Red signal is sent by the control system to the piezo driver to correct the piezo length and minimize error signal. Ideally error signal should be kept almost in zero however this is not the case. This plot shows how both signals are in phase, in our system when control signal is a growing function error is a decreasing function and vice versa. The fact that they seem to be proportional means the cavity piezo response is too slow for the control system to notice this change on time. This makes the system to oscillate around the locking point retracing the error signal back and forth.

Chapter 5

Conclusions and Future Work

This thesis has established the basis for the issues that must be resolved when designing the cavity that will be used inside the vacuum chamber of the Laboratorio de Óptica Cuántica de Rydberg. One of the main questions is how important is alignment for a near concentric resonator like this one, it was addressed theoretically in section 2.5 where an explanation was given of how a minor tilt on the mirrors causes a major change in the orientation of the optical axis making the fundamental mode coupling more difficult because the beam center at the mirrors moves away rapidly from the mirror center. Also, in section 2.1 it was shown that when approaching the concentric regime, the beam waist at the mirrors rapidly grows as a function of cavity length making diffraction losses to increase deteriorating coupling. Experimentally it was found that when getting near the concentric regime the cavity became highly sensitive to any kind of mirror displacement, even touching lightly the mirror mount screws would dramatically change coupling and alignment. In the present work effective mode matching for a smaller waist was not possible because of different aspects, first mode matching optics available had not enough effective aperture to focus the beam without truncating it significatively. Secondly more precise kinematic mirror mounts would help alignment in a nearest to concentric regime. However, this situation should also improve when we get a lenses mode matching system planned to focus a smaller waist. Despite this, the constructed system serves very precisely to achieve a waist very near to the desired of about $5\,\mu$m.

The cavity micrometric translational stage was very useful to tune cavity length and the piezo proved to be very effective for cavity length scanning, as shown in Figure 3.5. Also linearity of the length scanning around transmission peaks is seen in Figure 3.6

where sideband peaks appear both at the same distance.

Generation of sidebands for cavity locking was very robust when implementing the EOM, over previous not reported attempts of sideband generation by means of a double pass AOM configuration which provided error signals not as similar to the theory as the one obtained in this thesis in Figure 4.5. This error signal is ideal to lock the cavity length, however a faster response of the mechanical system is still needed as concluded in section 4.1.
As a general conclusion this work provided an insight into the difficulties that represent building a near concentric cavity, the important aspects to take into account and effective techniques for alignment and characterization for this type of resonators.

Future Work
For the reasons given above a future design should consider the following aspects:

1. A system to precisely adjust mirror tilt, once it is adjusted mirrors position can be fixed and coupling adjusted moving the cavity alignment mirrors or the mode matching lenses.

2. It is necessary to consider the size the waist acquires at the mirrors near the concentric limit to ensure that at least four times the waist fits within the mirrors surface. This will improve fundamental mode coupling avoiding diffraction ripples. By the same reasoning mode matching lenses should have an effective aperture which does not truncate the beam into a circular shape conserving its gaussian shape. It would be recommended but not necessary to have a precision translation mechanism for the focusing lens to improve waist position matching into the cavity easily without losing alignment and thus minimizing higher Laguerre-Gauss modes coupling.

3. A faster response of the system might be achieved by using piezo electrics with higher bandwidth and getting the piezo nearer to the cavity mirror. Also, the cavity length locking can be improved by a design which is more isolated from mechanical vibrations. Additionally, when placed inside the vacuum system, air currents will no longer affect the system and it will need less feedback from the control system improving cavity length locking. Moreover, in the future we would like to build a design compatible with vacuum that can be housed inside our science chamber where the atoms are cooled and trapped. One of the biggest drawbacks is ultra-high vacuum compatible designs should avoid complex mechanisms which cannot be effectively depressurized. Based on the aspects learned, the new design is considering the use of ring piezo stacks almost directly in contact with the mirrors to maximize simplicity and get a faster response from the system. It is also planned to implement a method to adjust delicately mirror position, then fix it and remove alignment pieces before introducing the cavity inside vacuum. To lock the cavity length, it is planned to use a laser with a 1020 nm wavelength that does not couple the Rubidium transitions used in the experiment. As it has been shown, when measuring cavity length in

section 3.2, two lasers with different frequency can be simultaneously resonant when they satisfy the condition that their difference in wavelengths is an integer multiple of the free spectral range which in this cavity is around 1500 MHz. Cavity length can then be locked with a non-resonant to the atomic sample frequency while using a laser resonant with the desired atomic transition simultaneously. We can adjust this resonant frequency in the order of MHz by varying cavity length within the piezo range. This is important since the magnitude of the usual detunings from atomic transitions used at the Laboratorio de Óptica Cuántica de Rydberg (Rydberg Quantum Optics Laboratory) is in the order of MHz.

Bibliography

[1] C. Gross and I. Bloch. Quantum simulations with ultracold atoms in optical lattices. *Science*, **357**, 2017. DOI: 10.1126/science.aal3837 (cited on page 1).

[2] F. Schäfer et al. Tools for quantum simulation with ultracold atoms in optical lattices. *Nat. Rev. Phys.*, 2020. DOI: 10.1038/s42254-020-0195-3 (cited on page 1).

[3] X. Zhang and J. Ye. Precision measurement and frequency metrology with ultracold atoms. *Natl. Sci. Rev.*, **3**, 2016. DOI: 10.1093/nsr/nww013 (cited on page 1).

[4] M. Saffman. Quantum computing with atomic qubits and Rydberg interactions: progress and challenges. *J. Phys. B. At. Mol. Opt.*, **49**, 2016. DOI: 10.1088/0953-4075/49/20/202001 (cited on page 1).

[5] T. Haensch and A. Schawlow. Cooling of gases by laser radiation. *Opt. Commun.*, **13**, 1975. DOI: 10.1016/0030-4018(75)90159-5 (cited on page 1).

[6] D. J. Wineland and W. M. Itano. Laser Cooling. *Phys. Today*, **40**, 1987 (cited on page 1).

[7] S. Chu et al. Three-dimensional viscous confinement and cooling of atoms by resonance radiation pressure. *Phys. Rev. Lett.*, **55**, 1985. DOI: 10.1103/PhysRevLett.55.48 (cited on page 1).

[8] R. J. Thompson, G. Rempe, and H. J. Kimble. Observation of normal-mode splitting for an atom in an optical cavity. *Phys. Rev. Lett.*, **68**, 1992. DOI: 10.1103/PhysRevLett.68.1132 (cited on page 1).

[9] S. Haroche. Cavity quantum electrodynamics: a review of Rydberg atom-microwave experiments on entanglement and decoherence. *AIP Conf. Proc.*, **464**, 1999. DOI: 10.1063/1.58235 (cited on page 1).

[10] J. Lim, H.-g. Lee, and J. Ahn. Review of cold Rydberg atoms and their applications. *J. Korean Phys. Soc.*, **63**, 2013. DOI: 10.3938/jkps.63.867 (cited on page 1).

[11] C. S. Adams, J. D. Pritchard, and J. P. Shaffer. Rydberg atom quantum technologies. *J. Phys. B At. Mol. Opt.*, **53**, 2020. DOI: 10.1088/1361-6455/ab52ef (cited on page 1).

[12] T. F. Gallagher. *Rydberg Atoms*. New York: Cambridge University Press, 1° edition, 1994 (cited on page 2).

[13] C. Cohen-Tannoudji, B. Diu, and F. Laloe. *Quantum mechanics*. Wiley, New York, 1978 (cited on page 2).

[14] A. Paris-Mandoki et al. Tailoring Rydberg interactions via Förster resonances: state combinations, hopping and angular dependence. *J. Phys. B: At. Mol. Opt. Phys.*, **49**. DOI: 10.1088/0953-4075/49/16/164001 (cited on page 2).

[15] C. Gerry and P. Knight. *Introductory Quantum Optics*. Cambridge University Press, 2004. DOI: 10.1017/CBO9780511791239 (cited on page 3).

[16] M. Tavis and F. W. Cummings. Exact solution for an N-molecule—radiation-field hamiltonian. *Phys. Rev.*, **170**, 1968. DOI: 10.1103/PhysRev.170.379 (cited on page 4).

[17] E. Hecht. *Optics*. Addison-Wesley, 1998 (cited on page 5).

[18] B. E. A. Saleh and M. C. Teich. *Fundamentals of photonics; 2nd ed.* Wiley series in pure and applied optics. Wiley, New York, NY, 2007 (cited on pages 5–7, 17).

[19] A. E. Siegman. *Lasers*. University Science Books, 1986 (cited on pages 10, 12, 15, 26).

[20] M. Suter and P. Dietiker. Calculation of the finesse of an ideal Fabry–Perot resonator. *Appl. Opt.*, **53**, 2014. DOI: 10.1364/AO.53.007004 (cited on page 16).

[21] N. Ismail et al. Fabry-Pérot resonator: spectral line shapes, generic and related Airy distributions, linewidths, finesses, and performance at low or frequency-dependent reflectivity. *Opt. Express*, **24**, 2016. DOI: 10.1364/OE.24.016366 (cited on page 19).

[22] D. Z. Anderson. Alignment of resonant optical cavities. *Appl. Opt.*, **23**, 1984. DOI: 10.1364/AO.23.002944 (cited on pages 24, 25, 27).

[23] R. Hauck, H. P. Kortz, and H. Weber. Misalignment sensitivity of optical resonators. *Appl. Opt.*, **19**, 1980. DOI: 10.1364/AO.19.000598 (cited on page 26).

[24] Y. You et al. Measurement of beam waist for an optical cavity based on Gouy phase. *Nucl. Instrum. and Methods Phys. Res. A*, **694**, 2012. DOI: 10.1016/j.nima.2012.07.022 (cited on page 30).

[25] M. Durand, Y. Wang, and J. Lawall. Accurate Gouy phase measurement in an astigmatic optical cavity. *Appl. Phys. B*, **108**, 2012. DOI: 10.1007/s00340-012-5147-x (cited on page 30).

[26] R. W. P. Drever et al. Laser phase and frequency stabilization using an optical resonator. *Appl. Phys. B*, **31**, 1983. DOI: 10.1007/BF00702605 (cited on page 34).

[27] E. D. Black. An introduction to Pound Drever Hall laser frequency stabilization. *Am. J. Phys.*, **69**, 2001. DOI: 10.1119/1.1286663 (cited on page 34).

[28] R. W. P. Drever et al. A gravity wave detector using optical cavity sensing. In *9th Int. Conf. Gen. Rel. and Grav.* 1980 (cited on page 34).